[redacted]

NASA CR-111784

N 71 1089

Final Report

TRIPLEXER FOR WIDEBAND VARACTOR FREQUENCY TRIPLER

By: B. M. SCHIFFMAN E. G. CRISTAL L. YOUNG D. PARKER

Prepared for:

NATIONAL AERONAUTICS AND SPACE ADMINISTRATION
LANGLEY RESEARCH CENTER
LANGLEY STATION
HAMPTON, VIRGINIA 23365

STANFORD RESEARCH INSTITUTE
Menlo Park, California 94025 · U.S.A.

STANFORD RESEARCH INSTITUTE
Menlo Park, California 94025 · U.S.A.

Final Report *June 1970*

TRIPLEXER FOR WIDEBAND VARACTOR FREQUENCY TRIPLER

By: B. M. SCHIFFMAN E. G. CRISTAL L. YOUNG D. PARKER

Prepared for:

NATIONAL AERONAUTICS AND SPACE ADMINISTRATION
LANGLEY RESEARCH CENTER
LANGLEY STATION
HAMPTON, VIRGINIA 23365

CONTRACT NAS 12-2165

SRI Project 8035

Approved:

CHARLES J. SCHOENS, *Director*
Electromagnetic Techniques Laboratory

RAY L. LEADABRAND, *Executive Director*
Electronics and Radio Sciences Division

Copy No. ...18...

ABSTRACT

This report describes a triplexer for a third harmonic varactor multiplier. Designed to cover the maximum bandwidth, that is one for which the third and fourth harmonic bands are contiguous, the triplexer and its associated harmonic rejection filters embody a wide range of microwave stripline filter design techniques. These include quarter wave stub, parallel-coupled and reentrant type resonators for bandstop filters, and interdigital and digital elliptic-type construction for bandpass filters. The triplexer consists of two diplexers composed of singly-terminated pseudo-complementary bandstop and bandpass filters with Chebyshev response. Test results on this device with respect to its triplexing function (excluding harmonic generation tests with a varactor) are given.

The impedance matching network for the varactor diode was designed using a computer optimization approach. The tripler efficiency was analyzed using a time-domain analysis program in which a punch-through diode characteristic was assumed.

The authors present a few experimental data on the tripler performance at spot frequencies, using stub tuners to approximate ideal matching conditions.

PURPOSE OF CONTRACT

The purpose of the contract is to design and fabricate wideband triplexers for tripler applications.

CONTENTS

ILLUSTRATIONS

ILLUSTRATIONS (Continued)

ILLUSTRATIONS (Concluded)

TABLES

I INTRODUCTION

This is the final report on a one-year research project for the Electronics Research Center, National Aeronautics and Space Administration. The objective of the contract was to develop a series of triplexers[1*] for third harmonic varactor multipliers for space applications as outlined in SRI Proposal ELU 69-5 (Revised).

During the course of the project after development of the first triplexer, and at the request of the sponsoring agency, effort was shifted from triplexer development to varactor impedance matching. According to this second approach bandstop harmonic rejection filters would be omitted as separate system components, but their function would be incorporated in the matching network.

This report describes a triplexer and two harmonic filters for a fundamental band centered on 0.75 GHz, and the results of a computerized technique for matching a varactor in the fundamental and third harmonic bands.

Cognizant technical personnel engaged on this project were Dr. A. I. Grayzel and Mr. Robert Minkoff of NASA and Drs. L. Young, E. G. Cristal, and D. Parker, and Mr. B. M. Schiffman of SRI.

---

[*] References are listed at the end of the report.

II TRIPLEXER FOR THIRD HARMONIC GENERATOR

A. General

The function of the triplexer is to physically separate and electrically isolate the input port (fundamental) from the output port (third harmonic) in a varactor frequency multiplier. At the same time, second and fourth harmonic frequencies are to be reflected to the source (varactor), while subharmonic and other nonharmonic frequencies are to be absorbed in a dummy load at the third triplexer port. Ideally the phase at the varactor of the reflected second, and possibly the fourth, harmonic should remain within certain bounds.

A block diagram is shown in Figure 1. It is a four-port consisting of an assembly of two (similar) diplexers and two bandstop filters. The diplexers consist of a bandstop and a bandpass filter connected in parallel, thus forming a three-port. Each diplexer and each bandstop filter was designed as an integrated unit, each with its own input and output connectors (Type N), and the four units were then connected as in Figure 1. A photograph of the assembled triplexer is shown in Figure 2.

B. Operating Frequency

The maximum relative bandwidth of a third harmonic generator is fixed by the requirement that the third and fourth harmonic bands associated with a given fundamental band do not overlap. The maximum relative bandwidth is therefore 2/7 or

$$w = 0.286 \quad .$$

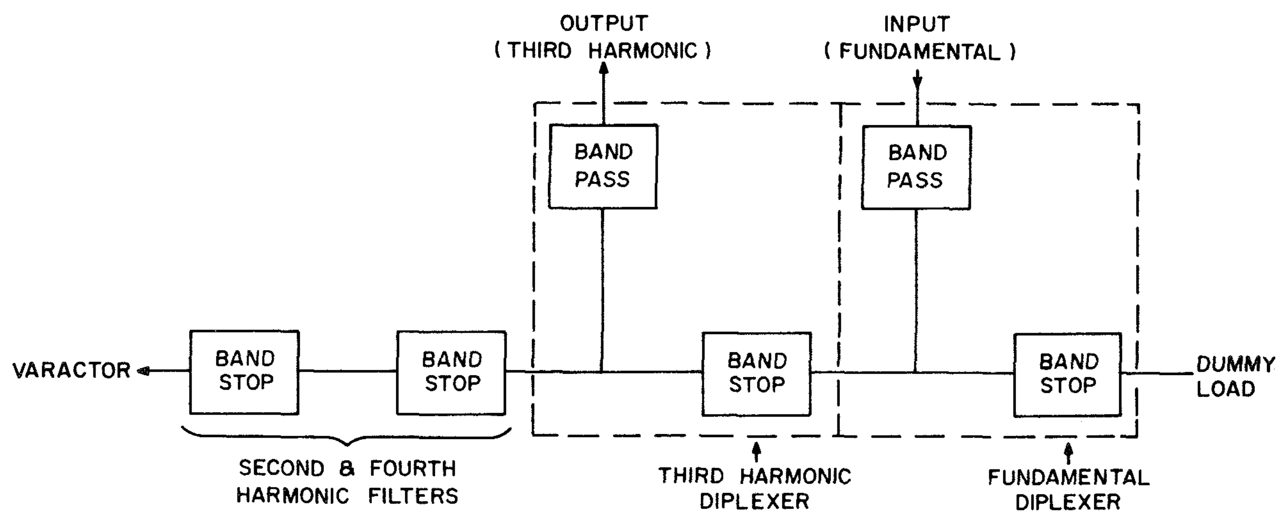

FIGURE 1 BLOCK DIAGRAM OF TRIPLEXER AND HARMONIC FILTERS

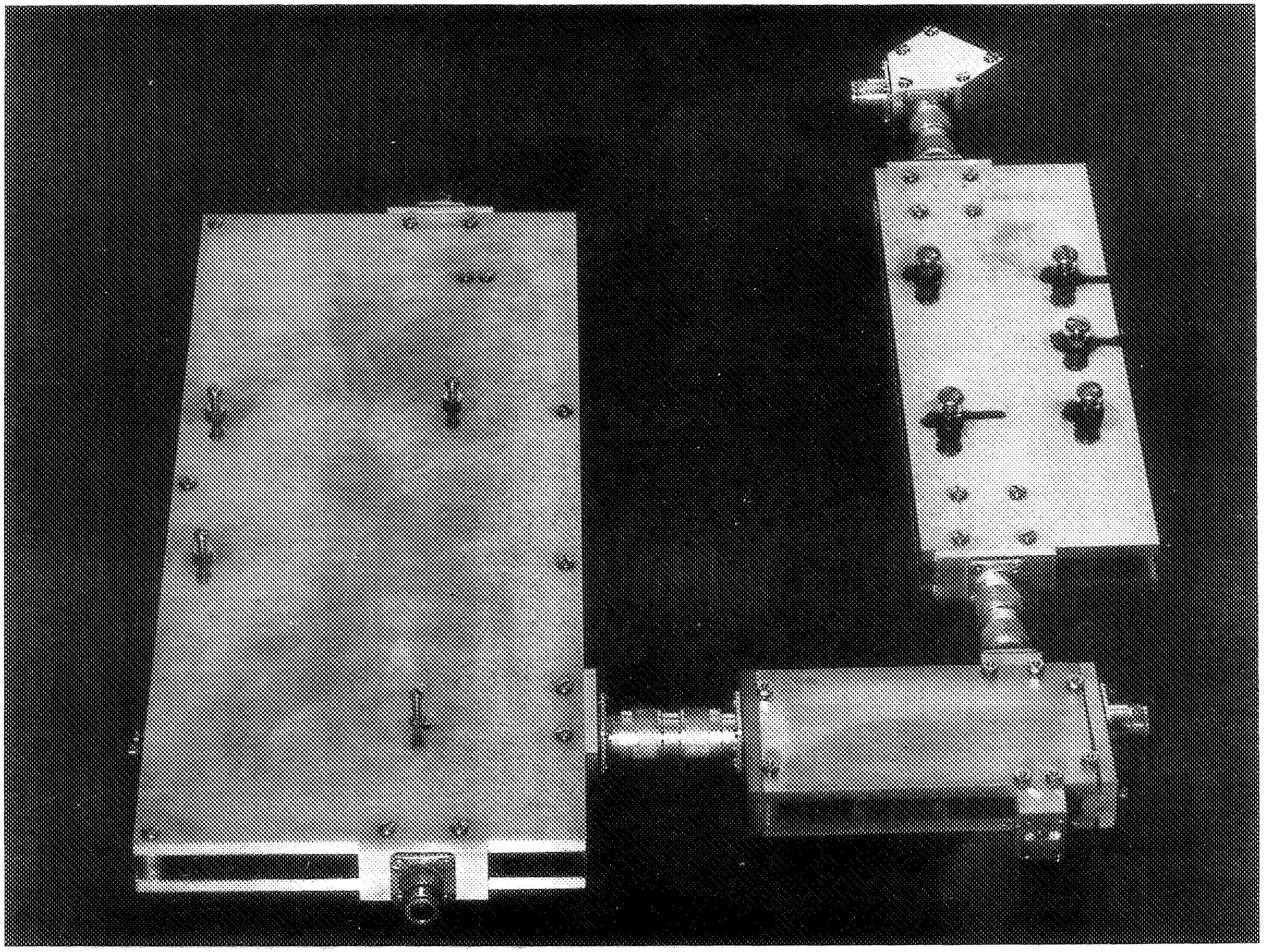

FIGURE 2 PHOTOGRAPH OF TRIPLEXER AND HARMONIC FILTERS

The center frequency for the fundamental band is 750 MHz, yielding the following harmonic bands:

Band	Harmonic	Frequency Range
I	Fundamental	643 to 857 MHz
II	Second	1286 to 1714 MHz
III	Third	1929 to 2571 MHz
IV	Fourth	2571 to 3429 MHz.

C. Design Considerations

In general, the performance requirements for the triplexer are not severe when each component is considered separately. Isolation between fundamental and third harmonic ports is to be 25 dB. Undesired harmonics are to be attenuated by at least 15 dB, of which at least 10 dB is to be accounted for by the bandstop filters. However, because the four bands are not, in general, widely separated (the third and fourth harmonic bands are actually contiguous), and because low insertion loss and good impedance match are also required, a certain amount of compromise was necessary. Many different configurations with different response characteristics were considered in the light of the above. Both theoretical and physical designs were worked out and then discarded because of practical considerations until, finally, the filters and diplexers described below were selected.

D. Fixing the Triplexer Response Characteristics

The overall response of the triplexer is determined by that of the two diplexers, and the way they are connected. First, a suitable response of the diplexer for the fundamental band (Band I) was found, and it was then seen that a scaled model of this diplexer would adequately cover the Band III requirements, yielding a satisfactory overall basic triplexer response. Figure 3 shows the measured frequency response of the two diplexers tested separately, and plotted on one graph. These are very close to theoretical. The solid lines (A) and (B) give the response of the bandpass and bandstop portions of the fundamental band diplexer respectively, and the dashed lines (C) and (D), the corresponding response of the third harmonic diplexer. In this figure, the harmonic band limits are also shown. Referring now to the block diagram of Figure 1 and the graphs of Figure 3, one could expect that a signal in the fundamental band would be channeled from the input through the fundamental and third harmonic diplexers to the varactor with negligible attenuation, as seen by curves (A) and (D) of Figure 3. Likewise, the signal should be well protected by about 30 dB or more isolation from power loss in the dummy load, as seen by curve (B), and by 25 dB or more from loss to the output port, as seen by curve (C). The third harmonic of the input generated in the varactor would then exit from the output port of the third harmonic diplexer with very low attenuation, as seen by curve (C). Curve (D) of Figure 3 shows that the third harmonic is well isolated by 30 dB or more from power loss to either the fundamental diplexer or the dummy load.

It should be noted that the order of connection of the two diplexers as shown in Figure 1 is important to the proper operation of the diplexers. If that order were reversed so that the diplexers were transposed, the third harmonic would exit from the fundamental diplexer input port because of the spurious pass band resulting from the distributed nature of filter elements in the diplexer. This spurious band, as shown in part by curve (A) of Figure 3, falls right in the third harmonic band as expected, but with the multiplexer connection of Figure 1, it should cause no trouble. For clarity, the responses of the second and fourth harmonic filters have been omitted from Figure 3, and these are dealt with later. Likewise, the actual overall response of the triplexer is presented later.

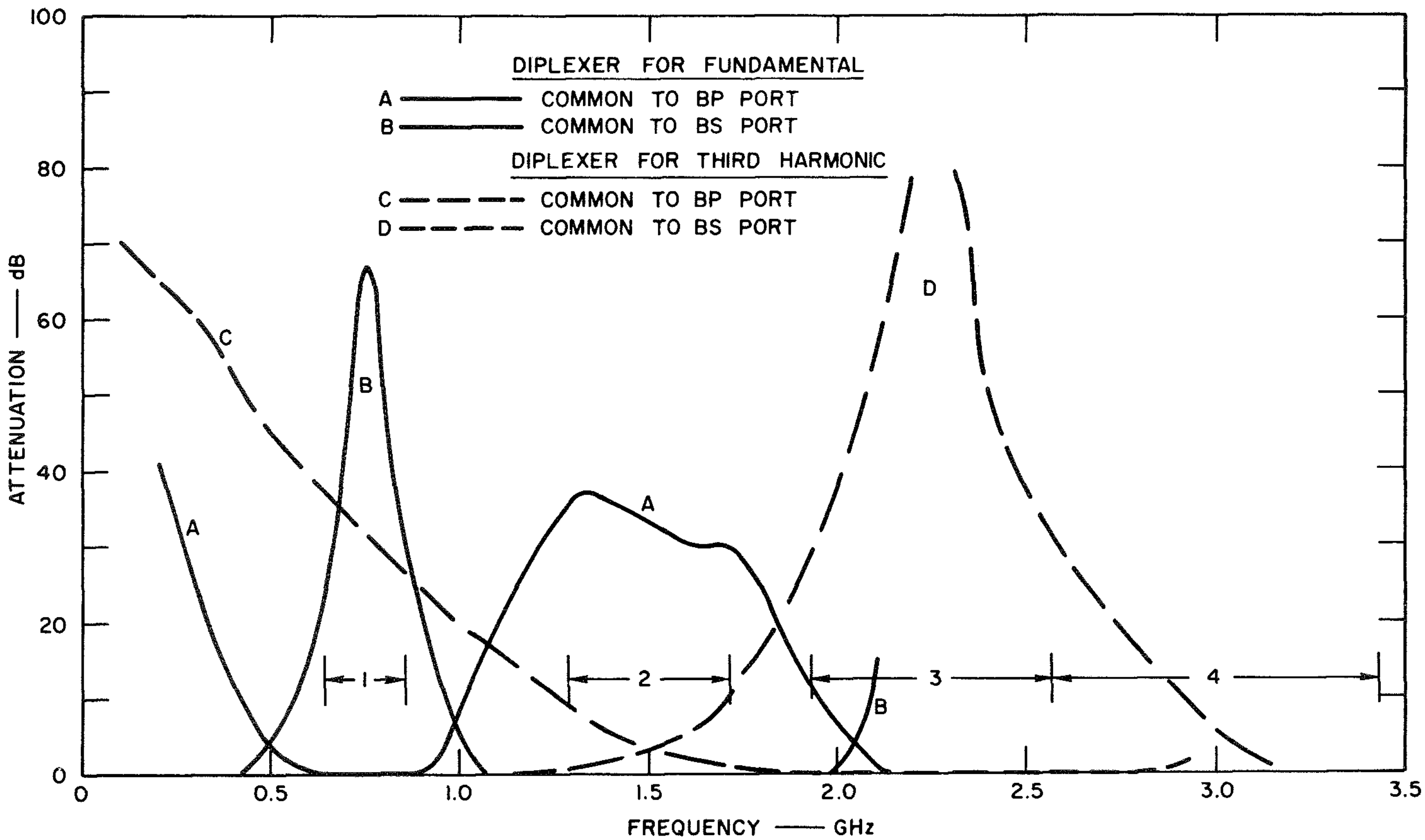

FIGURE 3 RESPONSE OF THE COMPONENT DIPLEXERS SUPERIMPOSED

E. Band I Diplexer

Here, a skeleton outline of the method of designing the diplexers is given, and later this is filled in with more details.

Starting with diplexer specifications, a canonical low-pass lumped element singly-terminated prototype is chosen [Figure 4(a)], and the 3-dB frequency (crossover frequency) of the prototype is determined. Then, scale factors Λ_{BP} and Λ_{BS} based on the prototype 3-dB frequency, the diplexer crossover frequency, and the diplexer center frequency are calculated for a bandpass and a bandstop filter [Figure 4(b)]. With these scale factors, normalized stub impedances are calculated from the low-pass prototype for the component filters of the diplexer [Figure 4(c)].

In Figure 4(c) the common port of the diplexer is shown to terminate in a resistance $R = 1$, in contrast with the prototype terminating value $g_4 = \infty$ in Figure 4(a). The reason for this seeming change is at the heart of the theory of diplexer design. The impedance of the diplexer at the common port ideally should be real and frequency invariant. To achieve this within practical limits, complementary filters are normally used. Such filters have the property that the real parts of the input admittances (in a shunt-connected diplexer) add to unity, and the imaginary parts add to zero. Singly terminated maximally flat filters have this property precisely, and singly-terminated Chebyshev filters closely approximate this condition when scaled for a 3-dB crossover frequency.[2]

That singly-terminated Chebyshev filters, when so employed, retain their excellent filtering properties is evident from the following argument. If the common port C is driven by a voltage generator with source resistance $R = 1$ for optimum power transfer, a nearly constant voltage appears across that port. This follows from the complementarity requirement placed on the component filters, which result in a real,

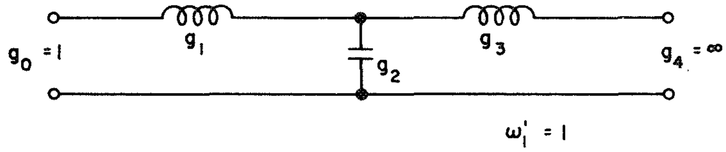

(a)

$$\Lambda_{BS} = \omega'_X \cot \frac{\pi}{2} \frac{f_X}{f_0}$$

$$\Lambda_{BP} = \omega'_X \tan \frac{\pi}{2} \frac{f_X}{f_0}$$

(b)

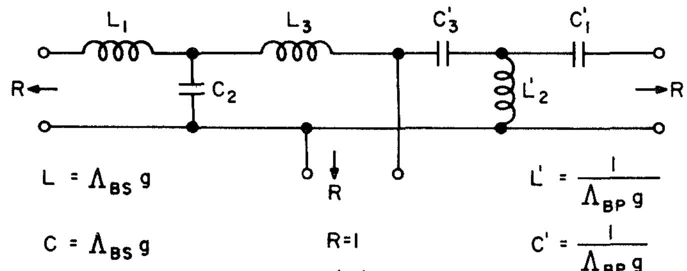

(c)

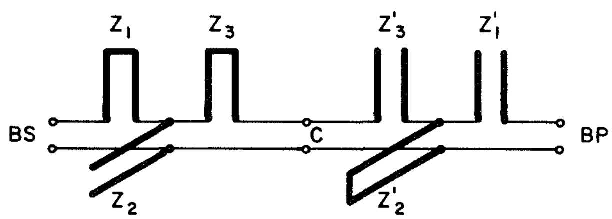

(d)

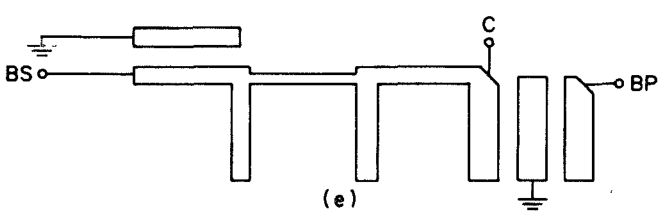

(e)

FIGURE 4 DEVELOPMENTAL OUTLINE OF DIPLEXER CIRCUIT

(a) Low-pass Lumped-element Prototype

(b) Scale Factors for Distributed-element (Transmission Line) Filters

(c) Basic Form of Diplexer Symbolic Elements

(d) Basic Form of Diplexer with Stubs

(e) Final Form of Diplexer

frequency-invariant input admittance $R \doteq 1$ at port C of the diplexer. Therefore each filter is separately driven by a constant voltage source. But this is precisely the requirement for Chebyshev behavior since, for the prototype filter, $g_4 = \infty$ corresponding to a short circuit, or more specifically a zero-impedance voltage generator. Thus, to the extent that complementarity exists in the component filters, the design response is preserved in the diplexer.

Returning now to the diplexer design, in Figure 4(c) inductors and capacitors represent short- and open-circuit stubs respectively as shown in Figure 4(d). The normalized element values L', C', L and C are then converted to the impedances of directly connected series and shunt quarter-wave resonators at a specific impedance level [Figure 4(d)], forming a bandpass and a bandstop filter. These two real but not very practical filter configurations (direct-connected stubs) are then separately altered to more practical forms [Figure 4(e)]. Here, the bandstop filter was modified to consist of two open-circuited stubs separated by a quarter-wave line and one parallel-coupled stub resonator. In addition, one length of line separates the first stub from the common junction with the bandpass filter. The bandpass filter was modified to consist of three coupled lines forming an interdigital filter.

1. Low-Pass Prototype and Basic Diplexer

Element values for the low-pass prototype [Figure 4(a)] were obtained from an inhouse computer program and are given in Table I. In Table I, g_0 and g_4 are conductances when applied to the circuit of Figure 4(a), and g_1 and g_3 are given in henrys and g_2 in farads. The 3-dB protype frequency (crossover frequency) for this filter is computed

Table I

ELEMENT VALUES FOR A LOW-PASS PROTOTYPE

No. of resonators	$n = 3$
Peak loss in pass band	$L_{Ar} = 0.3$ dB
Filter type	Chebyshev
$g_0 = 1$	
$g_1 = 0.68561$	
$g_2 = 1.24369$	
$g_3 = 1.25454$	
$g_4 = \infty$	

from the frequency response formula for n odd for a singly terminated Chebyshev filter:

$$\left.\frac{\omega'}{\omega_1'}\right|_{\omega' > \omega_1'} = \cosh\left\{\frac{1}{n}\cosh^{-1}\left[\frac{1}{\varepsilon}\left(\frac{g_0}{\text{Re } Y} - 1\right)\right]^{1/2}\right\} \quad . \tag{1}$$

Re Y is the real part of the input admittance of the component filters at frequency ω' as seen from the common port end, n is the number of elements, and ε is computed from

$$\varepsilon = \left[\text{antilog}_{10}\left(\frac{L_{Ar}}{10}\right)\right] - 1 \tag{2}$$

Substituting Re Y = 1/2 (normalized value), n = 3, and $\varepsilon = 0.0715$ [computed from $L_{Ar} = 0.3$ dB in Eq. (2)] we obtain $\leftarrow \omega_3'/\omega_1' = 1.229$. The scale parameters Λ in Figure 4(b) depend on the choice of crossover frequency f_x of the diplexer. Trial values of f_x were used to compute the frequency response of the diplexer, resulting in the choice of 1.0 GHz as the crossover frequency. This value yielded for the scale parameters,

$$\Lambda_{BS} = 0.7096$$

$$\Lambda_{BP} = 2.1286 \text{ (initial value)} \quad .$$

Using the formulas of Figure 4(c), the following normalized values of filter elements were obtained:

Table II

STUB VALUES NORMALIZED TO 1-OHM LEVEL

L_1	= 0.4865	C_1'	= 0.6852
C_2	= 0.8825	L_2'	= 0.3777
L_3	= 0.8902	C_3'	= 0.3745

The above element values are actually the admittances and impedances of open and short-circuited stubs normalized to a one-ohm level and do not represent inductance and capacitance values. When normalized to a 50-ohm level and converted to all impedances, the stub values of Figure 4(d) are given below:

Table III

STUB VALUES NORMALIZED TO 50-OHM LEVEL

Z_1	= 24.3	Z_1'	= 73.0
Z_2	= 27.6	Z_2'	= 18.9
Z_3	= 44.5	Z_3'	= 133.5

2. Bandstop Portion of Diplexer

The bandstop portion of the diplexer was then modified (see Figure 5) using Kuroda's identity,[4,5] by feeding three quarter-wave sections of 50-ohm transmission line from the BS port toward the common port C. The diplexer performance was not affected by this change, since

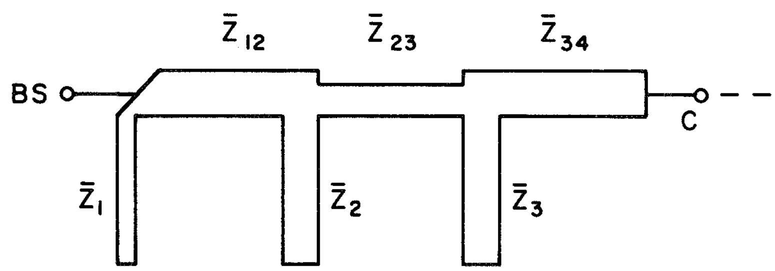

FIGURE 5 BANDSTOP PORTION OF DIPLEXER AFTER APPLICATION OF KURODA'S IDENTITY

the terminating impedances were not changed in any way, but the inserted quarter-wave lines served to conveniently separate directly connected stubs from each other, and in particular separate the BS and BP filters by a line section (part of the BS filter). In this configuration of the BS filter, not yet final, the following stub impedances $\bar{Z}_i$ and connecting line impedances $\bar{Z}_{ij}$ were obtained:

Table IV

VALUES OF STUB
AND CONNECTING LINE IMPEDANCES

$\bar{Z}_1$	= 252.8	$\bar{Z}_{12}$	= 62.3
$\bar{Z}_2$	= 71.3	$\bar{Z}_{23}$	= 79.9
$\bar{Z}_3$	= 55.4	$\bar{Z}_{34}$	= 76.7

Here, as before, stub 1 is near the BS port and stub 3 is near the common junction C.

The final modification of the BS filter is to change stub 1, which has a fairly high Z_0, to a parallel coupled resonator[6] stub as shown in Figure 4(e). Both the stub $\bar{Z}_1$ and its adjacent line section $\bar{Z}_{12}$ must be processed simultaneously. By allowing the coupled-line resonator to be asymmetrical, a wide choice of coupled-line parameters is possible, thereby allowing practical design values to be chosen. A convenient way of treating coupled-line design is to calculate the distributed capacitances of the lines normalized to the dielectric constant of the medium C_a/ϵ, C_b/ϵ and C_{ab}/ϵ, where the subscripts a and b refer to line and resonator, respectively, as shown in Figure 6. The formulas are

$$\frac{C_a}{\epsilon} = \frac{\eta_o}{\sqrt{\epsilon_r}} (Y_{12} + Y_1) - \frac{C_{ab}}{\epsilon} \qquad (3)$$

and

$$\frac{C_b}{\epsilon} = \frac{\sqrt{\epsilon_r}}{Y_1 \eta_o} \left(\frac{C_{ab}}{\epsilon}\right)^2 - \frac{C_{ab}}{\epsilon} \qquad (4)$$

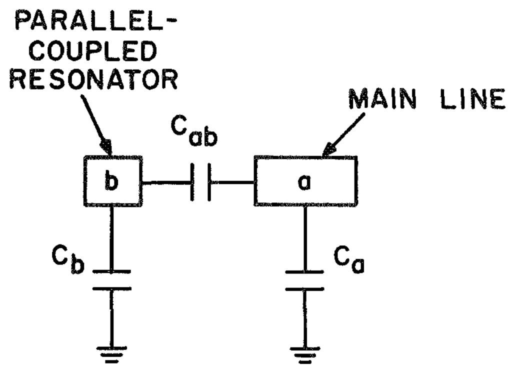

FIGURE 6 CIRCUIT CROSS SECTION OF PARALLEL-COUPLED RESONATOR SHOWING DISTRIBUTED CAPACITANCES

In the above formulas for coupled lines the original line $\overline{Z}_{12}$ and stub $\overline{Z}_1$ are given as normalized admittance Y_{12} and Y_1, ϵ has the value 0.0885 pf/cm, and ϵ_r is the relative dielectric constant. As long as C_a and C_b remain greater than zero, a wide choice of C_{ab} is possible. With $\sqrt{\epsilon_r} = 1$, the choice of $C_{ab}/\epsilon = 3.0$ yielded practical values for the coupled line capacities:

$$\frac{C_a}{\epsilon} = 4.534, \qquad \frac{C_b}{\epsilon} = 3.039, \qquad \frac{C_{ab}}{\epsilon} = 3.0 \quad .$$

Design curves for rectangular coupled lines between parallel gound planes were used to obtain dimensions of the lines,[7] as were design curves for the uncoupled portions of the BS filter, yielding the dimensions shown in Figure 7 for the bandstop portion of the Band I diplexer.

3. Design of the BP Filter

Many practical realizations of the direct connected stub BP filter of Figure 4(d) were investigated, but the interdigital configuration[8] appeared to be most compact and have least end effects that tend to degrade performance at high frequencies.

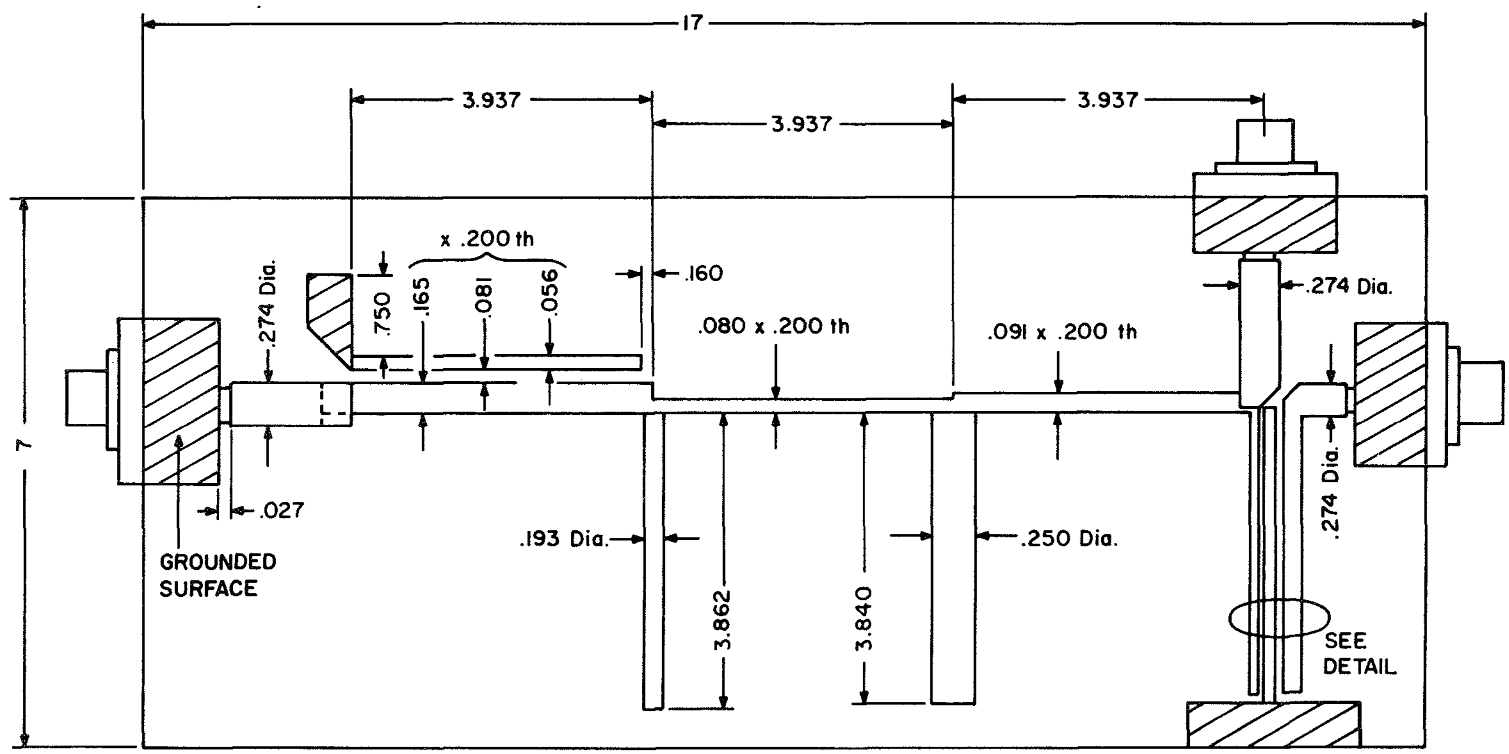

FIGURE 7(a) DRAWING OF DIPLEXER FOR BAND I SHOWING DIMENSIONS OF CIRCUIT ELEMENTS

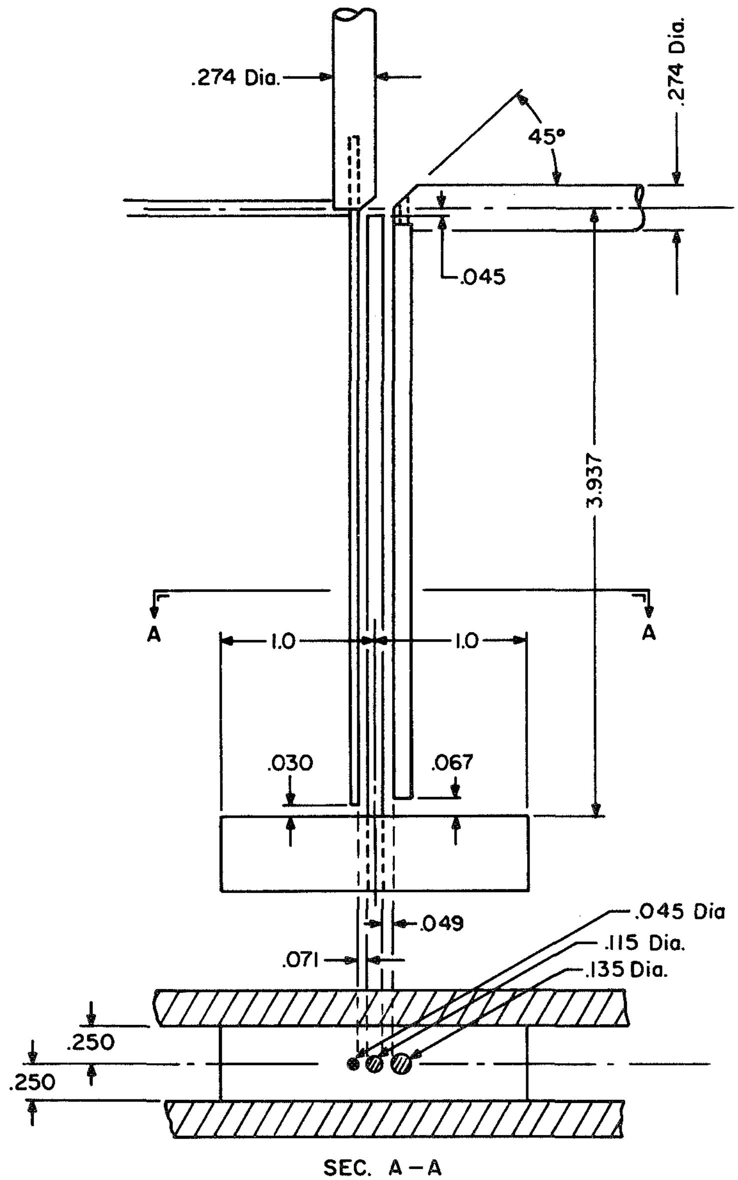

FIGURE 7(b) DRAWING OF DIPLEXER FOR BAND I SHOWING DIMENSIONS OF CIRCUIT ELEMENTS

The distributed capacitances of coupled lines are used in designing this portion. First, the distributed capacitances derived from the element values of Figure 4(c) are arranged in a 3 X 3 capacitance matrix,

$$\frac{1}{\epsilon}\,[C] \;=\; \frac{\eta_o}{Z_o}\begin{bmatrix} C_1' & -C_1' & 0 \\ -C_1' & C_1' + C_2' + C_3' & -C' \\ 0 & -C_3' & C_3' \end{bmatrix} \tag{5}$$

where the values of C_1', $C_2' = 1/L_2'$, and C_3' are given in Table II. Remembering that these are actually normalized admittance values, multiplication by the factor $\eta_o/Z_o = 7.534$ converts all elements to normalized capacitances C/ϵ for a 50-ohm system, a form well-suited to existing design graphs for coupled rods and bars. The matrix is interpreted to represent the capacitances of three coupled stubs as in Figure 4(e), where the self-capacitances of the stubs are given by the sum of the elements in their respective rows (or columns), and the interstub capacitances are given by the off-diagonal element. In general, we have

$$\frac{C_{gi}}{\epsilon} = \sum_j C_{ij} \tag{6}$$

$$\frac{\Delta C_{ij}}{\epsilon} = C_{ij} \quad . \tag{7}$$

The self capacitances C_g and the interstub capacitances ΔC are depicted in Figure 8 for the three-element interdigital structure. Note that

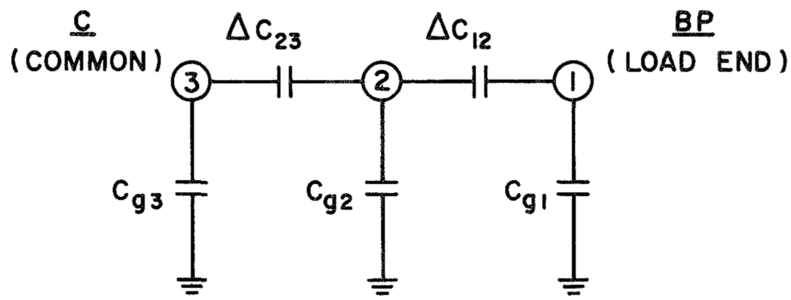

FIGURE 8 CIRCUIT CROSS SECTION OF INTERDIGITAL PORTION OF DIPLEXER

$C_{13} = 0$ in Eq. (5). This signifies stubs 1 and 3 are ideally fully isolated. Also, at the start stubs 1 and 3 have zero self capacitance ($\sum_j C_{ij} = 0$, $i = 1,3$) and the matrix can not directly yield a realizable three-element interdigital filter. (A reentrant type design may still be realizable but, because of its greater bulk and end effects, was not considered to be a good solution.)

The next step is to multiply the inner row and column by a transformer ratio $N < 1$, yielding a realizable C-matrix for an interdigital filter.[8] The effect is the same as post- and pre-multiplying the C-matrix by a transformer matrix, which has the effect of changing the internal impedance level of the filter while preserving the impedance match at each end. Of course, too small a transformer ratio will yield a negative self-capacitance for the center stub, again resulting in a non-realizable C-matrix.

Using Table II and Eq. (5), we first obtain

$$\frac{1}{\varepsilon}[C] = \begin{bmatrix} 5.162 & -5.162 & 0 \\ -5.162 & 27.928 & -2.825 \\ 0 & -2.821 & 2.821 \end{bmatrix}$$

After several trial values of transformer ration N, a value of N = 0.42 gave the C-matrix

$$\begin{bmatrix} 5.162 & -2.168 & 0 \\ -2.168 & 4.927 & -1.185 \\ 0 & -1.185 & 2.821 \end{bmatrix}$$

The self and interstub capacitances calculated from this C-matrix yielded practical dimensions for three coupled cylindrical rods between ground planes spaced one half inch apart. The rod diameters and their spacings for this initial design were obtained from design curves for coupled cylindrical rods,[9] and are given below.

Table V

INITIAL ROD DIAMETERS AND SPACINGS OF I.D.

Rod	Diameter (inches)	Spacing (clear gap)
1	0.135	
2	0.096	0.056
3	0.045	0.078

It will be noted that these dimensions are slightly different from those in Figure 7, which gives the final design dimensions for the Band I diplexer. How the final dimensions were worked out is explained below.

4. Tests on Band I Diplexer

The component BS and BP filters were tested separately and then as a unit, during which adjustments were made. Adjustments on the BS filter consisted of reducing resonator lengths and adding tuning screws at their open circuit ends, and then tuning the resonators to 750 MHz, the center of the stop band. An automatic network analyzer was used to display the real part of the input admittance at the common junction of the separate filters. The BS filter appeared well behaved, with Y_{in} approximating unity on a normalized basis in the pass bands and zero in the stop band, and having a value of approximately 0.5 at crossover frequencies (500 and 1000 MHz). Here, measurements of VSWR would not be applicable in testing a single filter.

The BP filter required considerably more attention. It was found that the initial interdigital filter (ID) did not have correct behavior of the real part of Y_{in}. However by adjusting the spacings of the coupled rods, and also tilting them so that they were no longer parallel, it was possible to obtain the desired behavior of R_eY_{in}. However, it was then found that the bandwidth was contracted by about 7.6 percent as measured between the 3-dB points (no meaningful measurement of bandwidth was possible until the correct behavior of R_eY_{in} was obtained). Then by returning to the low-pass prototype and applying a new scale factor Λ_{BP} computed for an appropriately wider bandwidth (7.6 percent wider) a revised C-matrix was written. The new scale factor is $\Lambda_{BP} = 1.959$ (compared with a value of 2.129 in initial design). A transformer ratio of $n = 0.47$ allowed a redesign of the interdigital filter in which only the center resonator and resonator spacings needed to be altered. The C-matrix became

$$\begin{bmatrix} 5.609 & -2.636 & 0 \\ -2.636 & 5.971 & -1.441 \\ 0 & -1.441 & 3.066 \end{bmatrix}$$

yielding self and interstub distributed capacitances as follows.

Table VI

DISTRIBUTED CAPACITANCES OF I.D.

$\frac{C_{g1}}{\epsilon} = 2.97$	$\frac{\Delta C_{12}}{\epsilon} = 2.63$
$\frac{C_{g2}}{\epsilon} = 1.89$	$\frac{\Delta C_{23}}{\epsilon} = 1.44$
$\frac{C_{g3}}{\epsilon} = 1.63$	

A new rod diameter for the center stub and new stub spacings were found from design curves for coupled rods[9] as shown in Figure 7(b). The spacings were, however, again adjusted in magnitude and tilt during testing to obtain $R_e Y_{in}$ approximately equal to unity in the pass band, as described earlier. The response curve of Figure 3 for the fundamental band (curves A and B) were obtained after all adjustments were made. Insertion loss in the fundamental band (643 - 857 MHz) did not exceed 0.2 dB as measured between the C and BP terminals. The VSWR of the diplexer for Band I is shown in Figure 9 in the range 0.2 to 2.0 GHz, as seen at the C port. The VSWR curves at the BP (input) port and at the BS (dummy load) port are shown in Figure 10.

The effects of a severe mismatch in either the BP port or the BS port as seen at the C port are shown in Figure 11, where the respective ports (BP and BS) were each successively left open-circuited, but with a load on the other port. The ability of the diplexer to separate the frequency bands is clearly seen in these curves.

A photograph of the Band I diplexer with cover plate removed is shown in Figure 12.

F. Band III Diplexer

The Band III diplexer was made as a scaled down version of the Band I diplexer in all respects, except for the ground plane spacing, which was kept the same. Curves C and D of Figure 3 are test results, but are very close to curves that were scaled from curves A and B by a factor of three (not shown in Figure 3), except for the peaks in the stop band. A dimensioned drawing of the essential features of the Band III diplexer is shown in Figure 13, and a photograph of this device with cover plate removed is shown in Figure 14.

Although the electrical circuits of the two diplexers are similar, lessons learned with respect to adjusting the spacing and tilting of the ID portion of the diplexer were applied in the mechanical design of the Band III diplexer. The stub nearest the common junction was made non-adjustable, while provision was made so that the center stub and the stub at the BP junction could be moved and then fixed in the optimum positions. The method of mounting allowed both a change in the inter-stub spacing and a tilt of the stubs so they are no longer parallel, as shown in Figure 13. Trimming was done by observing pass band VSWR of

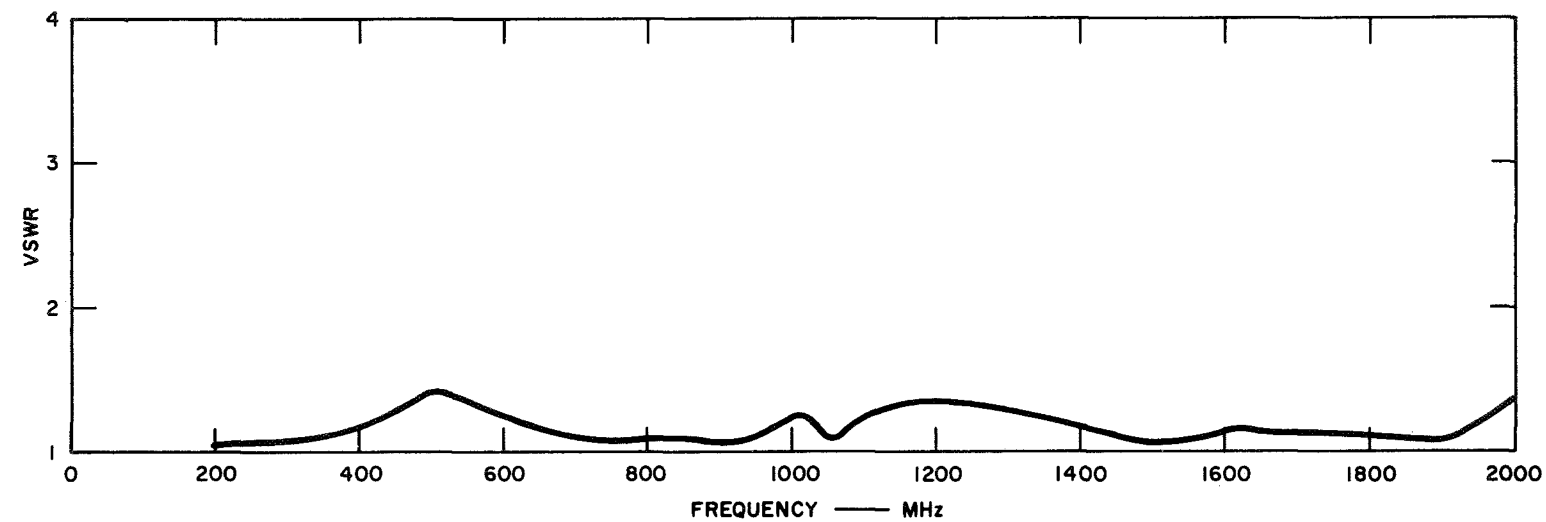

FIGURE 9 VSWR OF BAND I DIPLEXER AT THE COMMON (C) PORT

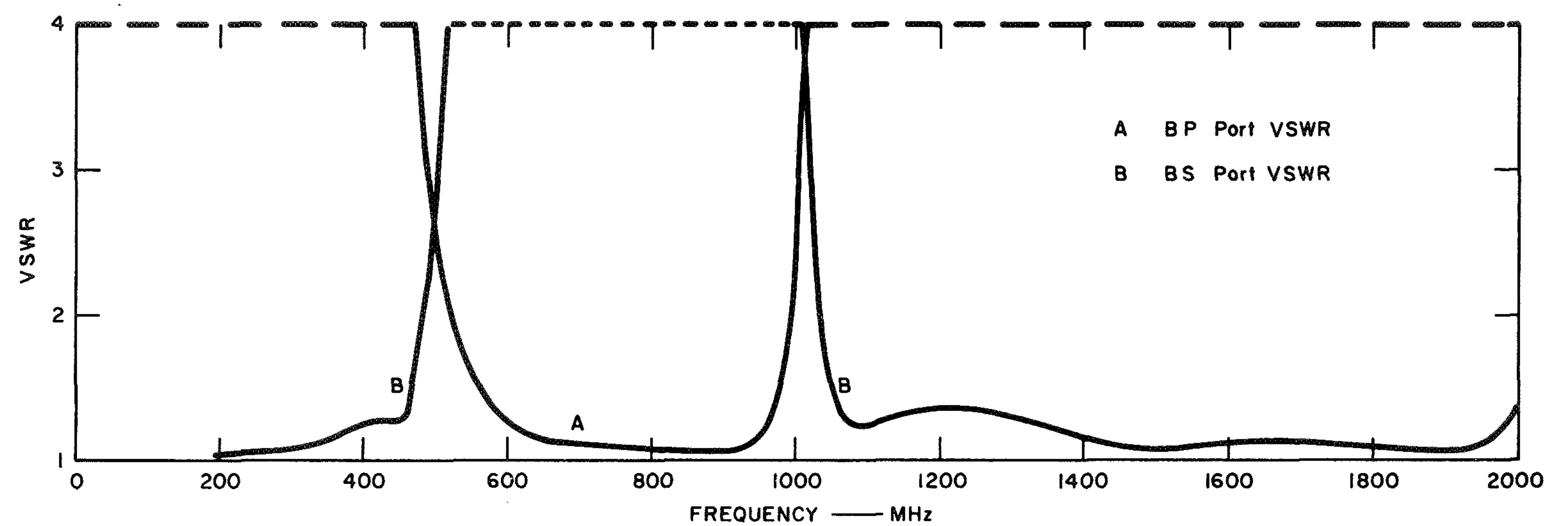

FIGURE 10 VSWR OF BAND I DIPLEXER AT THE BANDSTOP (BS) AND BANDPASS (BP) PORTS (CURVES A AND B RESPECTIVELY)

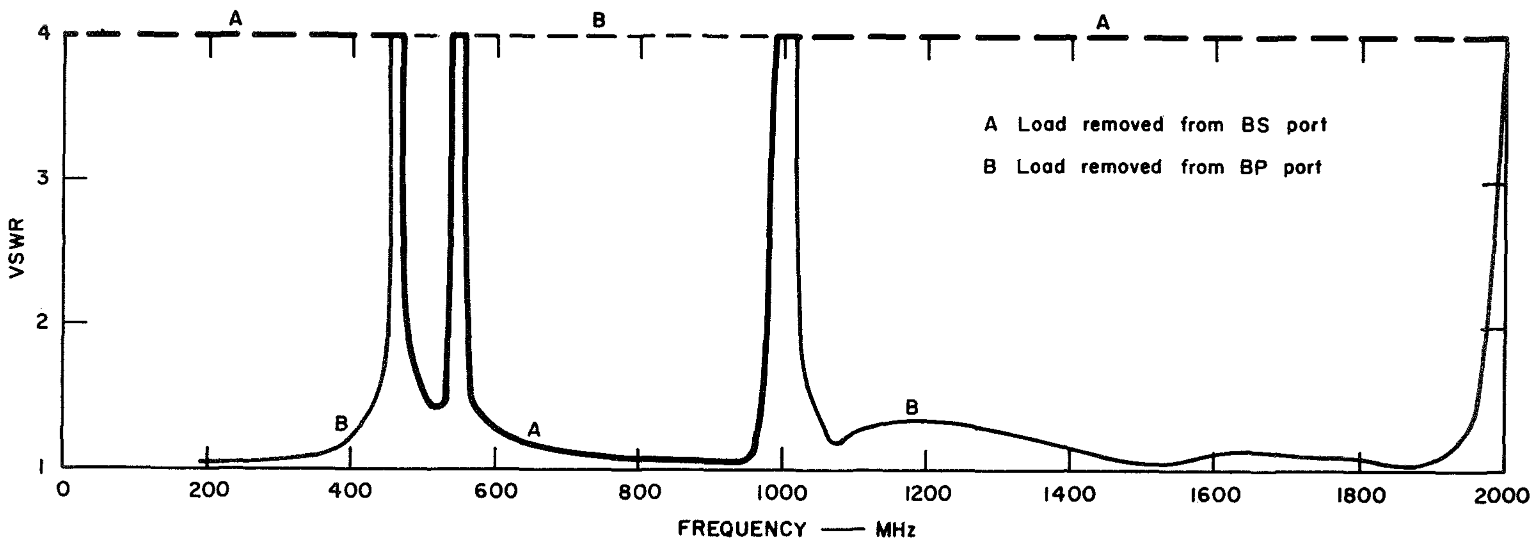

FIGURE 11 VSWR OF BAND I DIPLEXER AT THE COMMON PORT WITH THE BP AND BS PORTS OPEN (CURVES A AND B RESPECTIVELY)

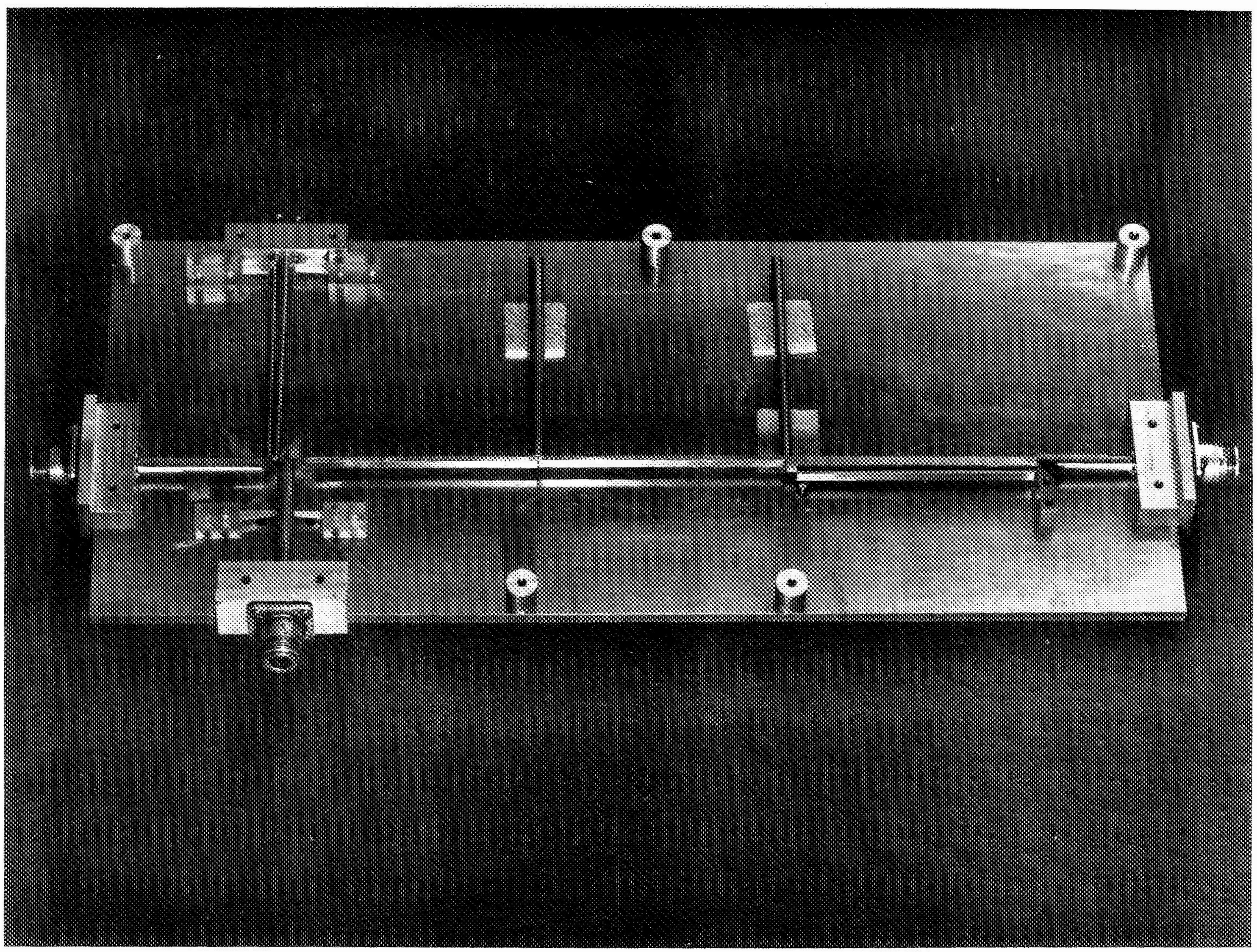

FIGURE 12 PHOTOGRAPH OF DIPLEXER FOR BAND I WITH COVER PLATE REMOVED

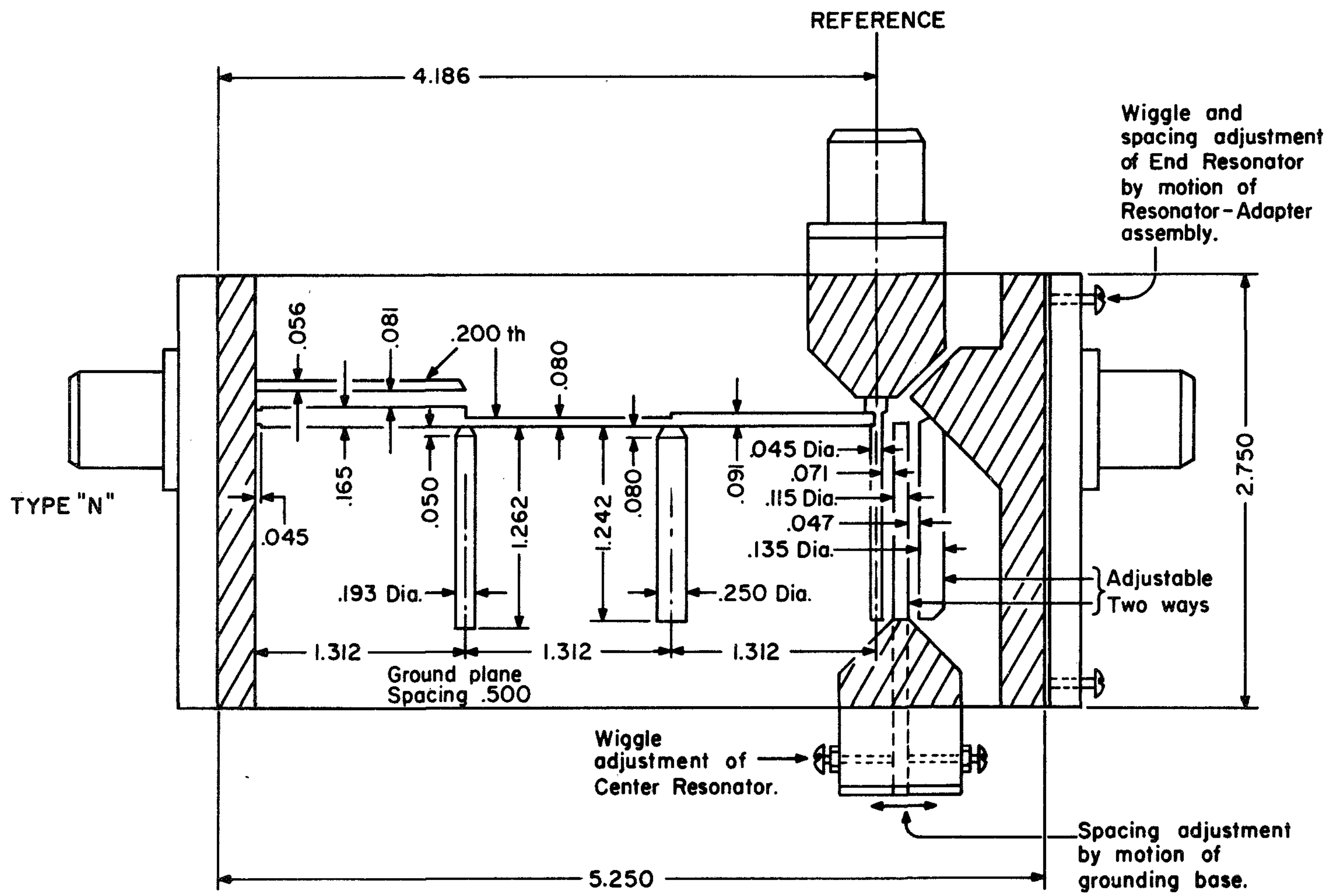

FIGURE 13 DRAWING OF THE BAND III DIPLEXER WITH DIMENSIONS OF CIRCUIT ELEMENTS

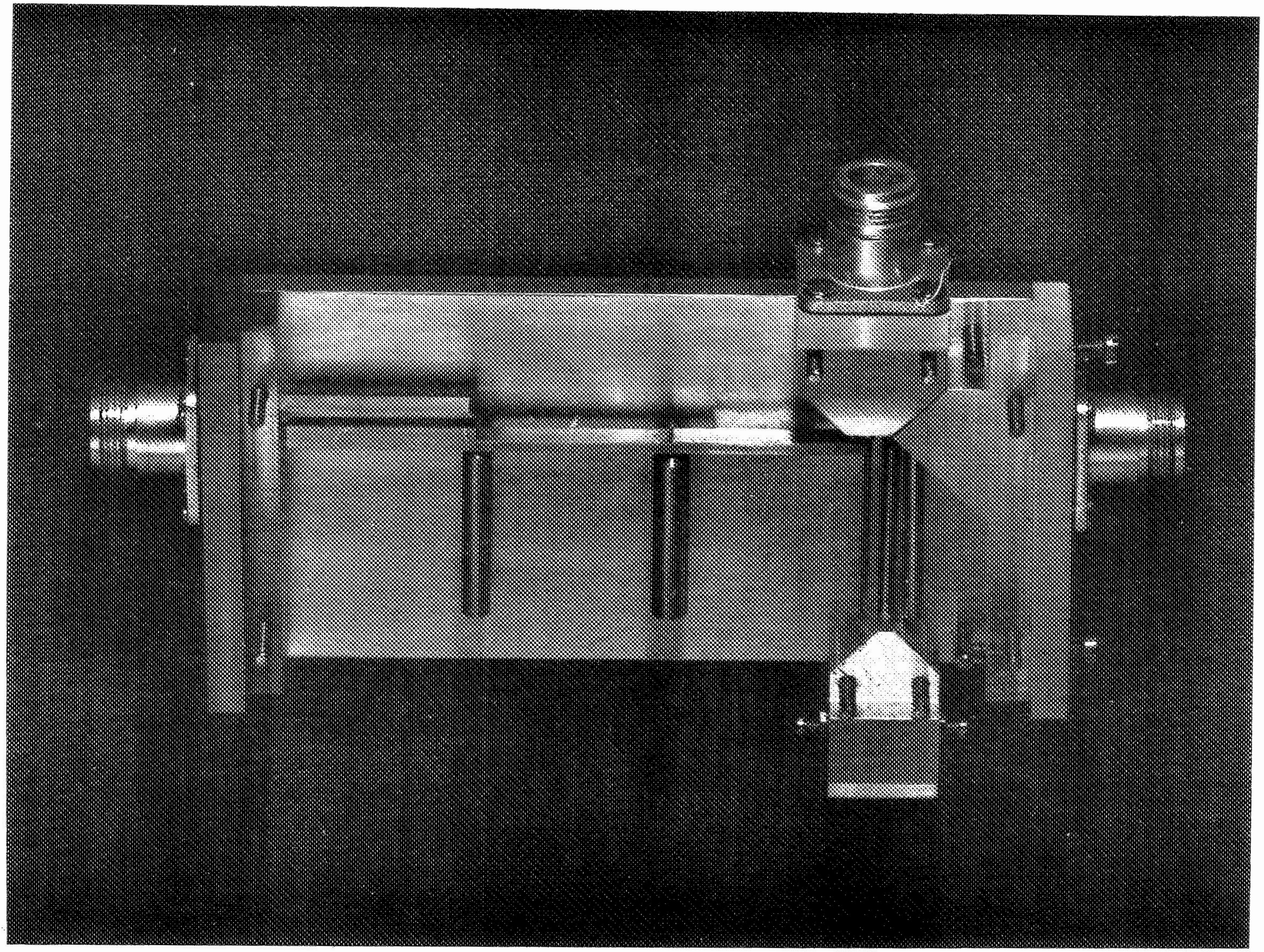

FIGURE 14 PHOTOGRAPH OF THE BAND III DIPLEXER WITH COVER PLATE REMOVED

the complete diplexer on a continuously swept basis. A VSWR curve for the common port of the Band III diplexer is shown in Figure 15. Although not generally as well matched as the Band I diplexer, a fairly good match is achieved in the third harmonic band, and an excellent match in the fundamental band and its surroundings.

G. Harmonic Rejection Filters

1. Band II Bandstop Filter

The second harmonic bandstop filter was designed to provide at least 10 dB attenuation in the range 1286-1714 MHz, and to be well matched in the fundamental and third harmonic bands. A five-element Chebyshev low-pass prototype with pass-band ripple of 0.01 dB was found to be well suited for this task. Unlike the component filters of the diplexers, the harmonic filters are of the doubly-terminated type.

A special requirement of a harmonic filter for a varactor multiplier is that the phase of the reflected wave (in the stop band) at the varactor terminal be contained within certain bounds. Excess line length between varactor and harmonic filter must therefore be avoided. Now in order to make the Band II filter simple in form, quarter-wave line sections are fed into it, but from one end only, in keeping with the above restriction. The feed end for the line sections is the one opposite the varactor terminal.

The low-pass prototype and the element values are shown in Figure 16(a). A scale factor of $\Lambda = 0.371$ converts these values to admittance and impedance values of a bandstop filter normalized to one ohm, as shown in Figure 16(b). Here, as before, the lumped-element form symbolizes a bandstop filter consisting of series short-circuit stubs and shunt open-circuit stubs. When four quarter-wave lines are fed in from the right end we obtain the all-shunt stub realization of

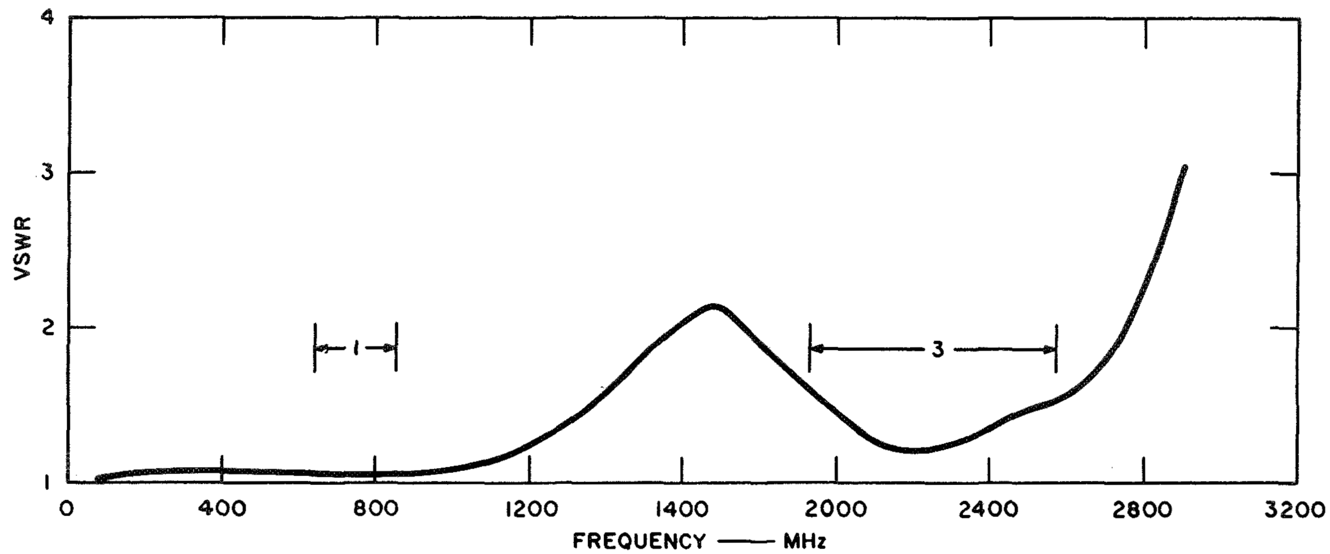

FIGURE 15 VSWR OF THE BAND III DIPLEXER AT THE COMMON PORT

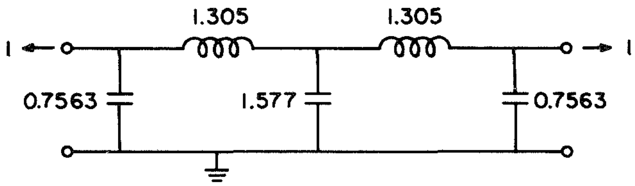

(a)

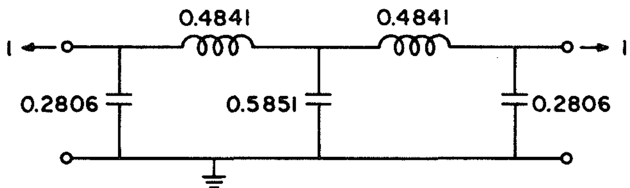

(b)

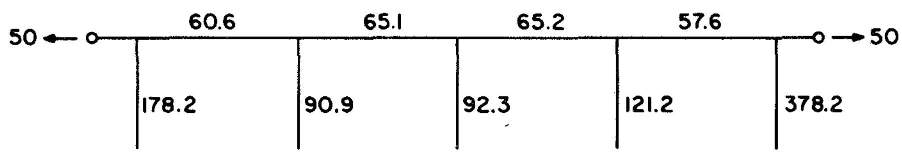

(c)

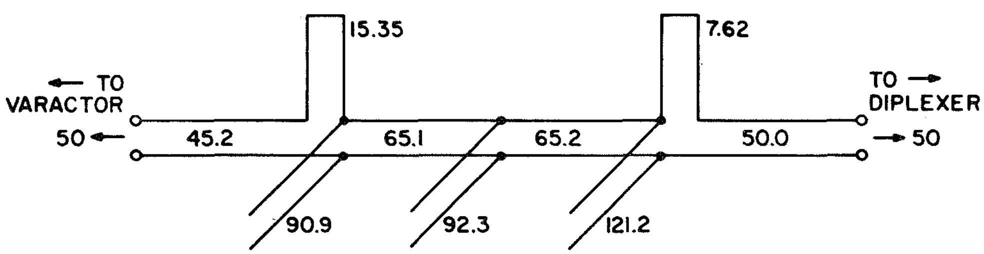

(d)

FIGURE 16 CIRCUIT DEVELOPMENT OF BAND II BANDSTOP FILTER

(a) Low-pass Prototype and Element Values
(b) Bandstop Filter and Element Values Normalized To One Ω
(c) All-Shunt Stub Form of Bandstop Filter with Line Sections Fed from Right End
(d) Modified Filter with End Sections Realizable as Reentrant Resonators

Figure 16(c). Since the end stubs are somewhat difficult to realize (178.2 ohms and 378.2 ohms), the filter is modified to the circuit of Figure 16(d). The series short circuit stub and the end line section near each port are now easily realized as reentrant line sections,[10] as shown in the detail drawing of the second harmonc filter in Figure 17. A photograph of the filter (cover plate removed) is shown in Figure 18.

The measured insertion loss curve for this filter is shown in Figure 19 and its VSWR curve in Figure 20. The filter met the attenuation specification at the edges of the second harmonic band very nicely, although VSWR in the pass band is higher than expected. The reason for this is not known.

2. Band IV Bandstop Filter

The fourth harmonic band is contiguous with the third harmonic band and a steep attenuation slope is required for this bandstop filter. An elliptic filter is therefore a natural choice. To keep the design down to a reasonable amount of complexity, an elliptic filter of order 6 was chosen.[11] A design labeled C0605c with modular angle $\theta = 40$ degrees was chosen for performance and practical realizability in digital elliptic filter[12] format. The 5 in the filter label signifies 5 percent reflection in the pass band. The modular angle relates directly to skirt steepness and inversely to minimum attenuation in the stop band A_s. In this case $A_s = 50.6$ dB. The element values for the low-pass prototype are shown in Figure 21(a). Here choice of scale factor depended more on physical realizability than on bandwidth coverage. Choosing $\Lambda = 1.0$ (100 percent bandwidth) yielded a practical design. An internal schematic view of the digital elliptic filter circuit is shown in Figure 21(b) for bars between parallel ground planes (not shown). The bars are open circuited at the far end and the reentrant coaxial lines are short circuited at the far end.

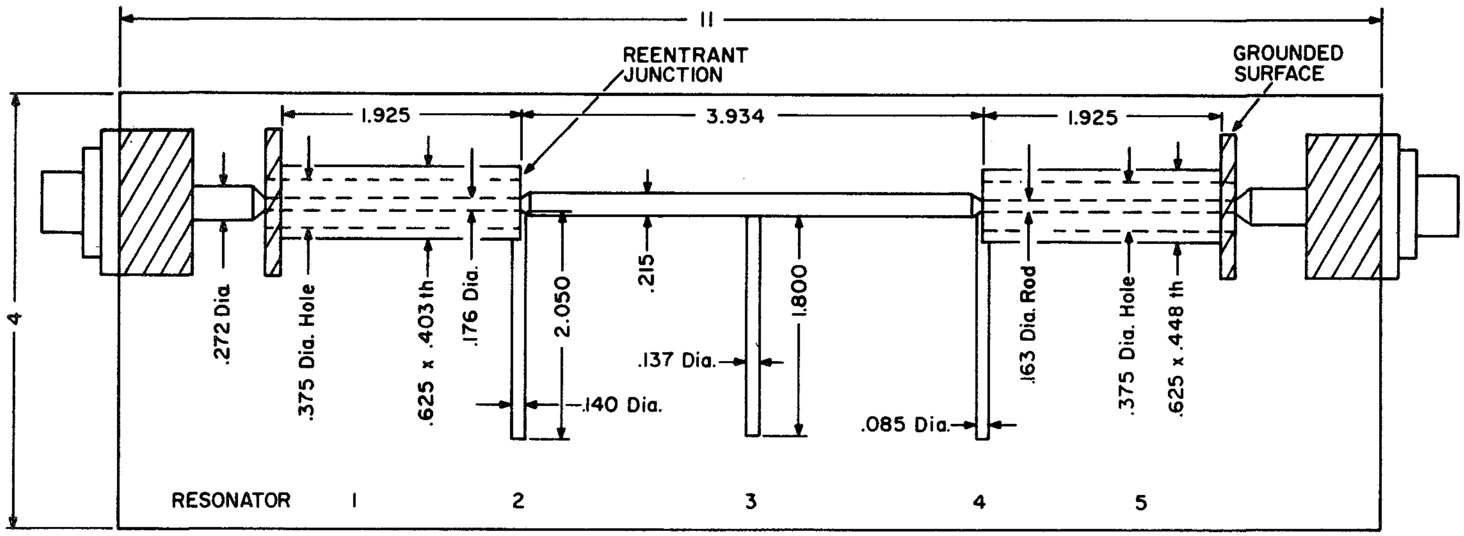

FIGURE 17 DRAWING OF BAND II BANDSTOP FILTER

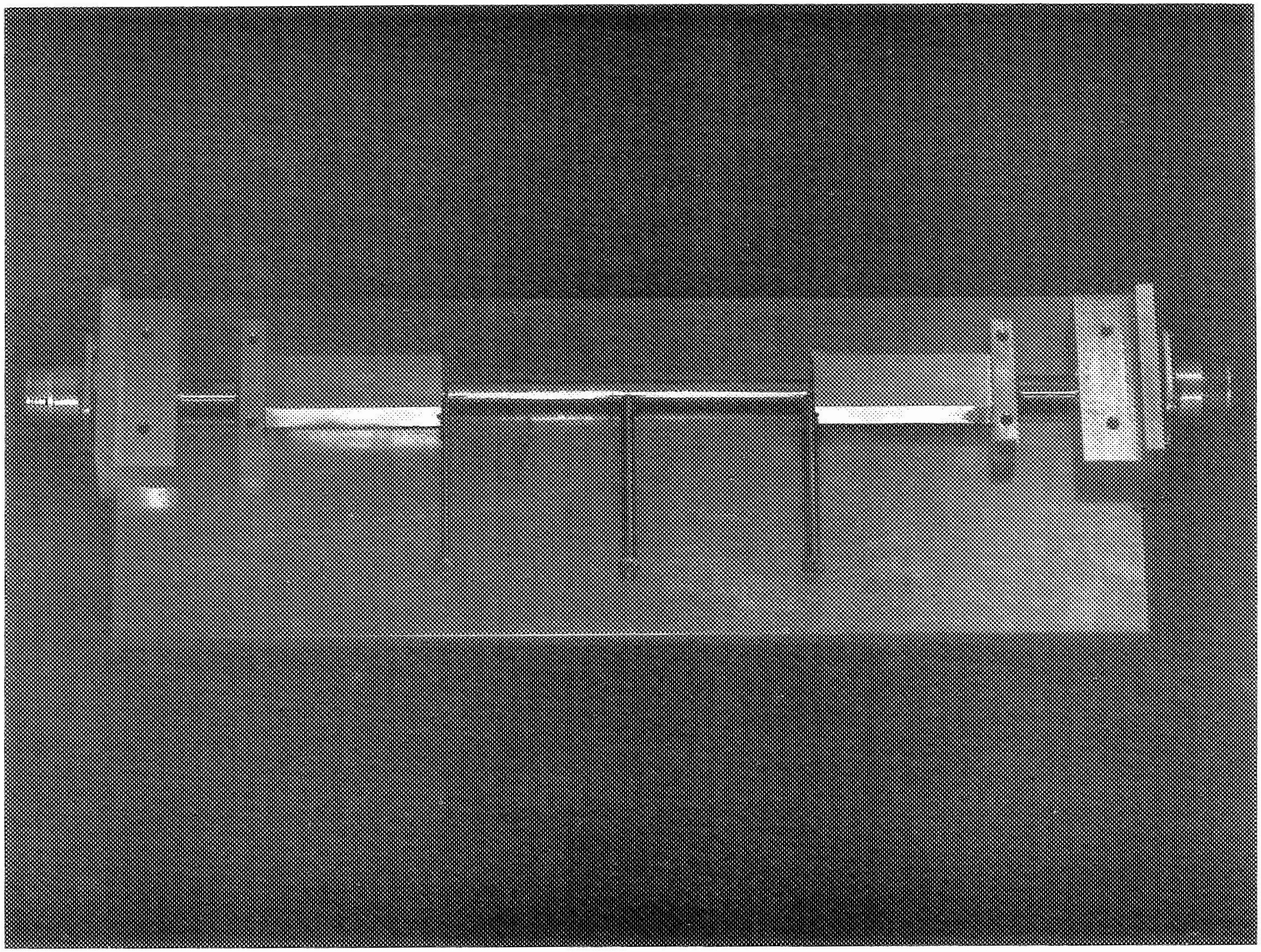

FIGURE 18 PHOTOGRAPH OF BAND II FILTER WITH COVER PLATE REMOVED

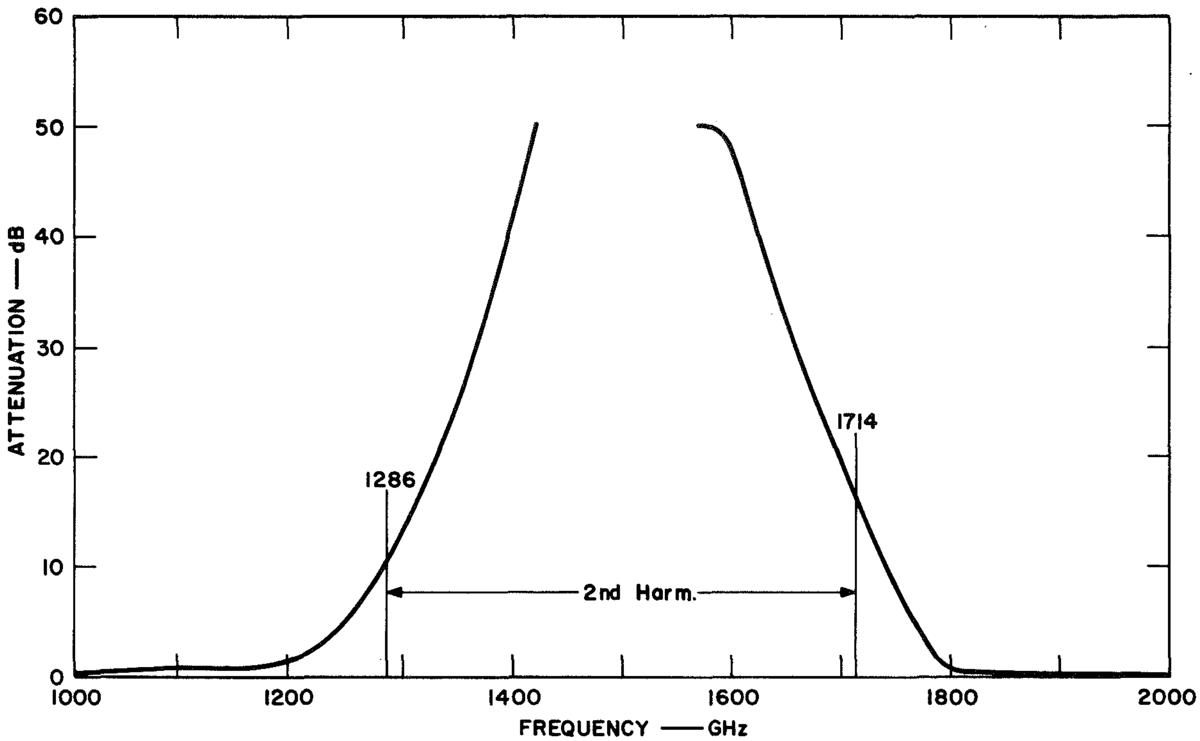

FIGURE 19 ATTENUATION RESPONSE OF BAND II FILTER

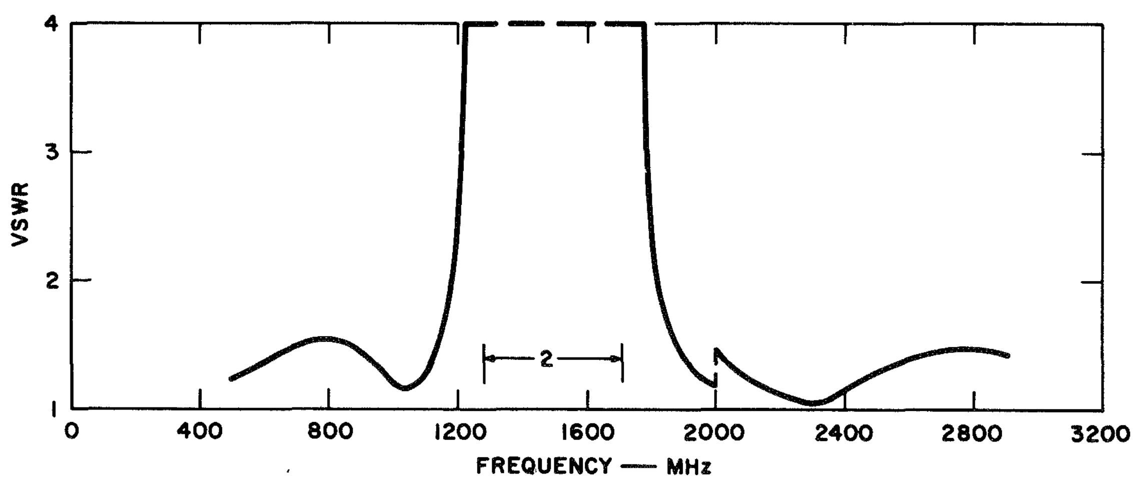

FIGURE 20 VSWR OF BAND II FILTER

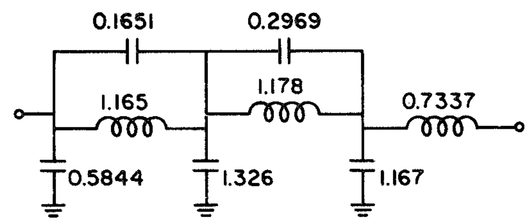

(a)

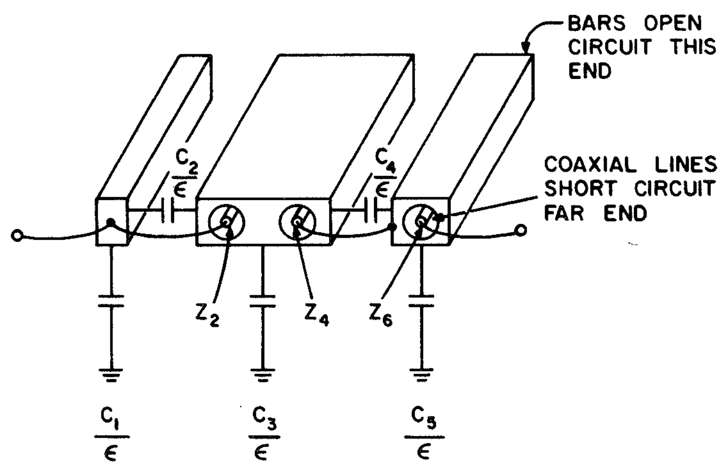

(b)

FIGURE 21 BAND IV BANDSTOP FILTER

(a) Lumped Element Low-pass Prototype

(b) Digital Elliptic Realization of Bandstop Filter

When the L values of Figure 21(a) are scaled by Λ and multiplied by the system Z_o (50 ohms) we obtain directly the impedances of the coaxial lines of the digital elliptic filter. Thus

$$Z_2 = 58.3 \qquad Z_4 = 58.9 \qquad Z_6 = 36.7$$

all in ohms. Next when the C values of Figure 21(a) are scaled by Λ and multiplied by $\eta_o/Z_o = 7.534$ we obtain directly the distributed capacitances C/ε of the coupled rectangular bars,[7] as follows:

$$C_1/\varepsilon = 4.403$$

$$C_2/\varepsilon = 1.244$$

$$C_3/\varepsilon = 9.990$$

$$C_4/\varepsilon = 2.237$$

$$C_5/\varepsilon = 8.792$$

The final design dimensions are shown in Figure 22. Note that the coaxial lines are dielectric filled, thereby permitting room for metal tuning slugs, rather than fixed short circuits. The vertical ground wall was brought near the right hand bar (Figure 21), and allowance was made for its contribution to C_5/ε. A similar treatment could have been given C_1/ε, but this bar was already fairly thin. The open circuit bar ends and the sheer drop in the ground planes at the bar ends were trimmed back twice during testing from 0.574 to 0.508 inch to bring the skirt of attenuation as close as possible to the third harmonic band upper edge.

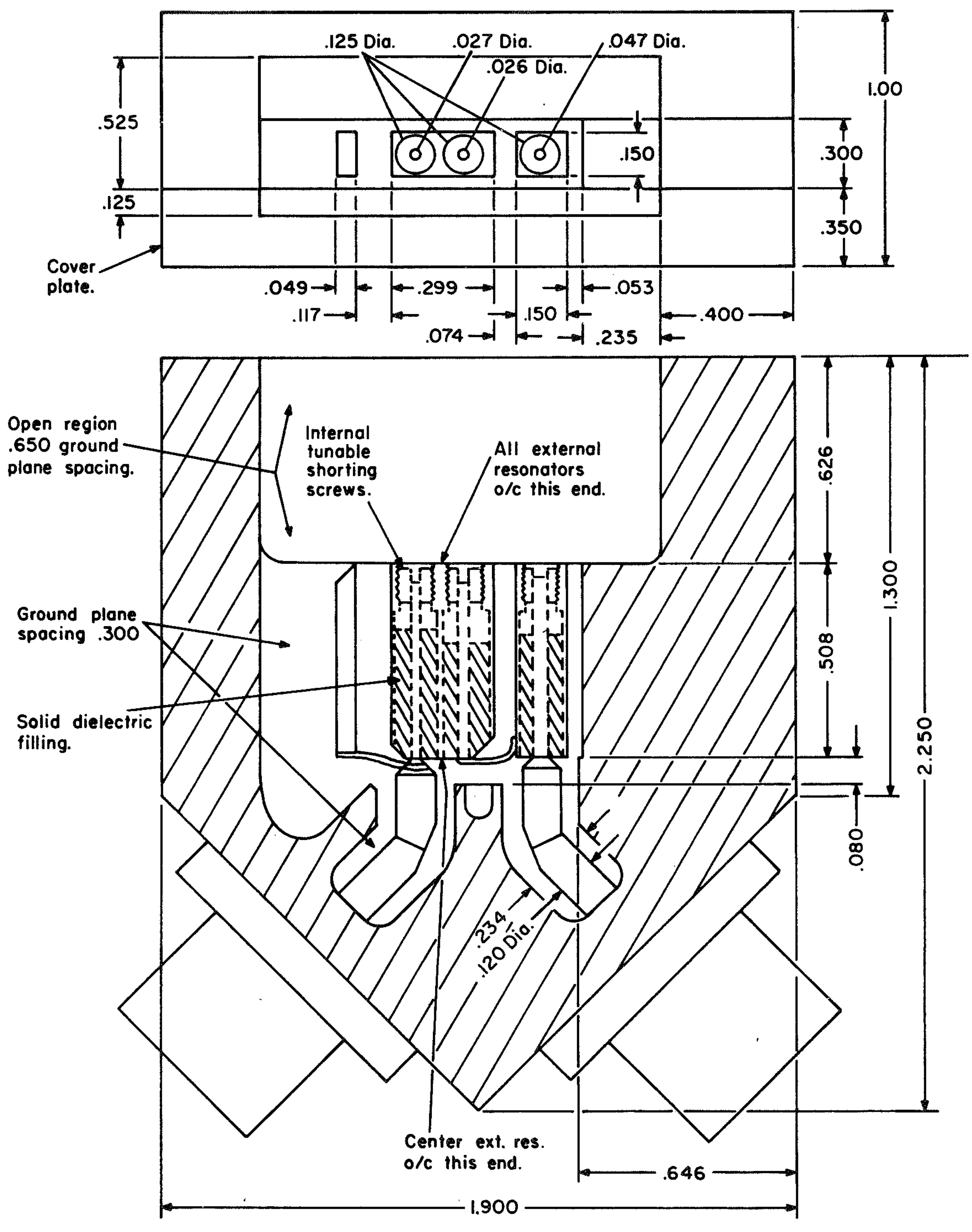

FIGURE 22 DRAWING OF BAND IV BANDSTOP FILTER

The VSWR and attenuation response of the Band IV filter are shown in Figure 23 in the region of the third and fourth harmonics. A photo of this filter is shown in Figure 24.

H. Test Results on the Triplexer System

Up to this point each component of the system was separately described and test results pertaining only to that component were given. Here results on the triplexer and the complete assembly of triplexer and two bandstop filters are given. The block diagram, Figure 1, and photo, Figure 2, show the way the components are assembled. In the case of the triplexer alone, the two bandstop filters are removed and the common port of the Band III diplexer becomes the varactor port.

Figure 25 shows the attenuation and VSWR of the triplexer alone, from the varactor port (input) to the fundamental port (output), covering more than four harmonically related bands. Here the test signal passes through the bandstop part of the Band III diplexer and the bandpass part of the fundamental diplexer. The two ports are well isolated from each other in the second, third, and fourth harmonic bands, as well as for subharmonics. When the second and fourth harmonic filters are added to the test setup, the curves of Figure 26 result. The VSWR increases sharply in these two harmonic bands, as one would expect. Some interaction appears to have occurred in the lower portion of the third harmonic band. However, the moderate values of VSWR in that region in both Figure 25 and Figure 26 are at variance with such a result. Some anomalous behavior of the test instrumentation could have been the cause of the apparent sudden drop in attenuation.

Figure 27 shows the response of the triplexer when the third harmonic port is the output, and the varactor port is the input. Here the two ports are well isolated in the fundamental band. In Figure 28 the two

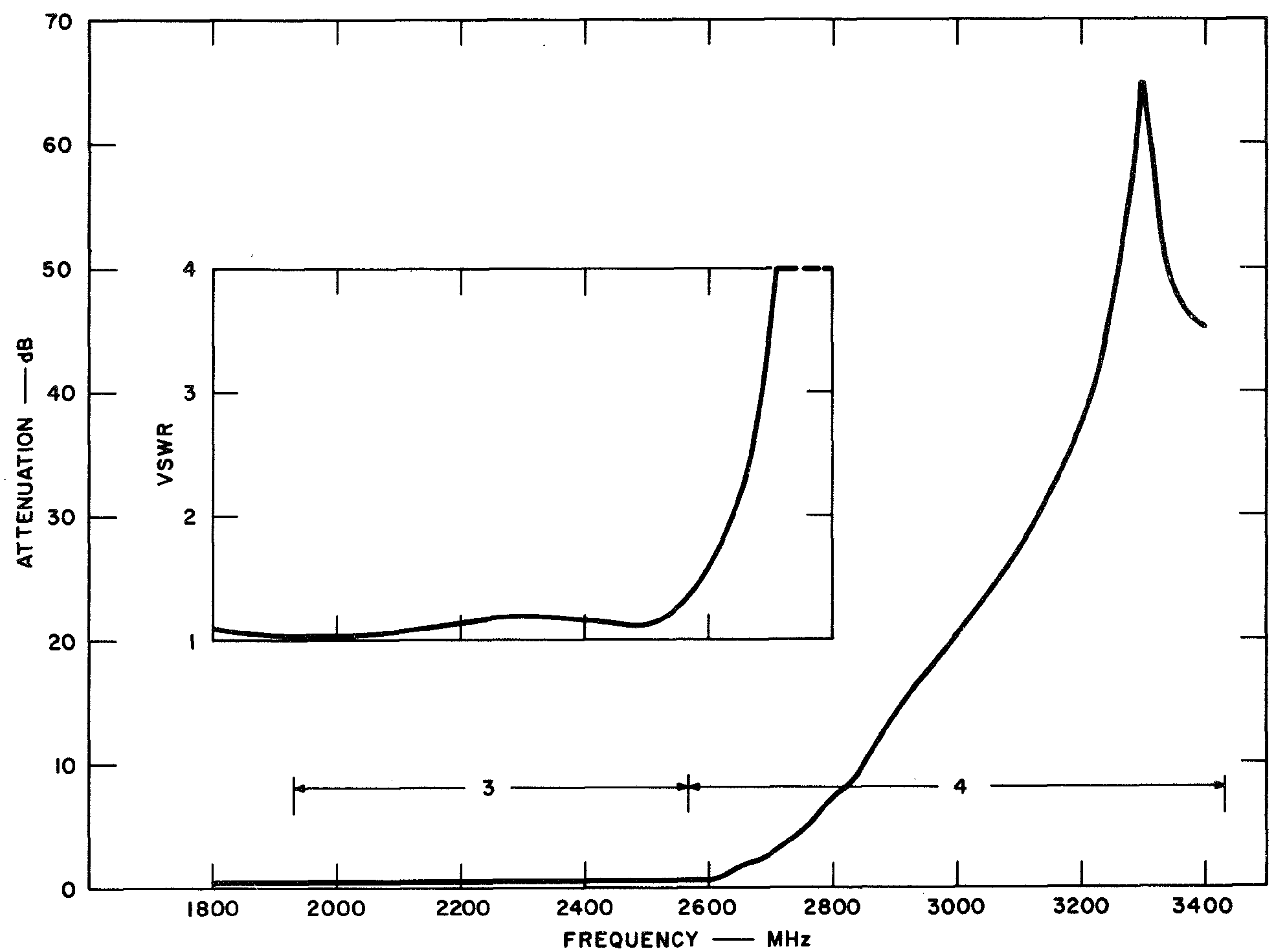

FIGURE 23 RESPONSE OF BAND IV FILTER

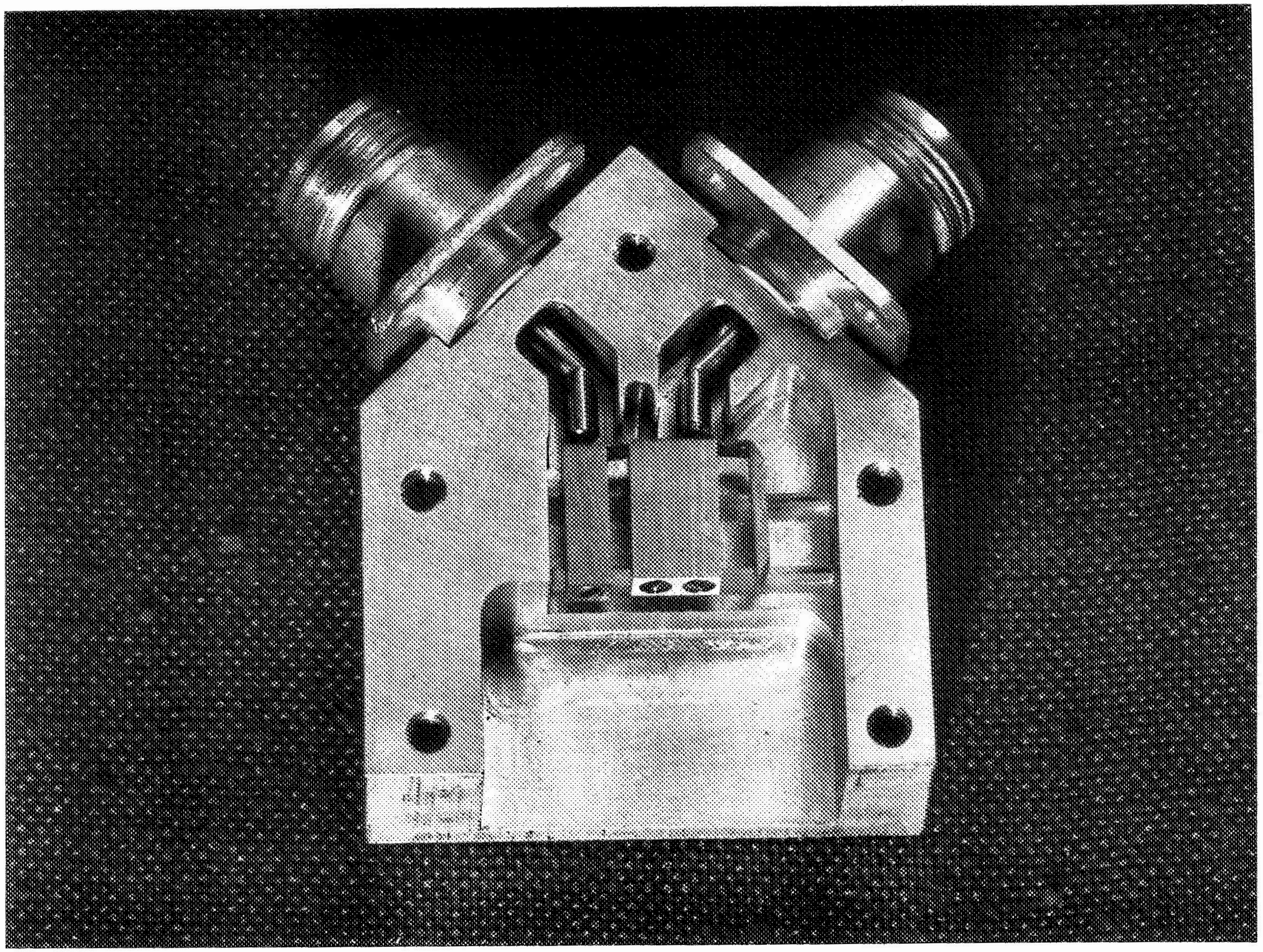

FIGURE 24 PHOTOGRAPH OF BAND IV FILTER WITH COVER PLATE REMOVED

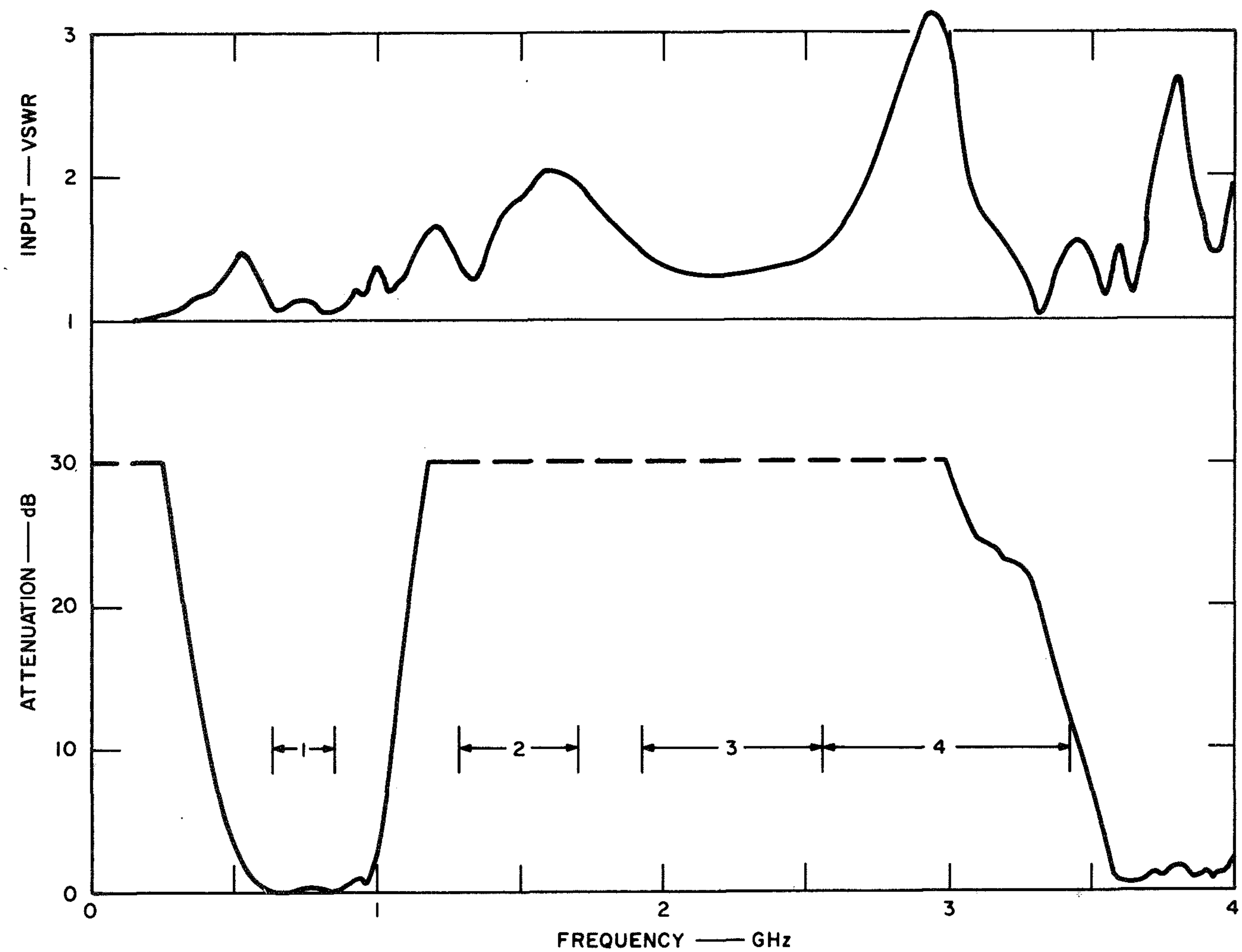

FIGURE 25 RESPONSE OF TRIPLEXER ONLY (BAND II AND BAND IV FILTERS OMITTED). Input is varactor port; Output is fundamental port (See Figure 1).

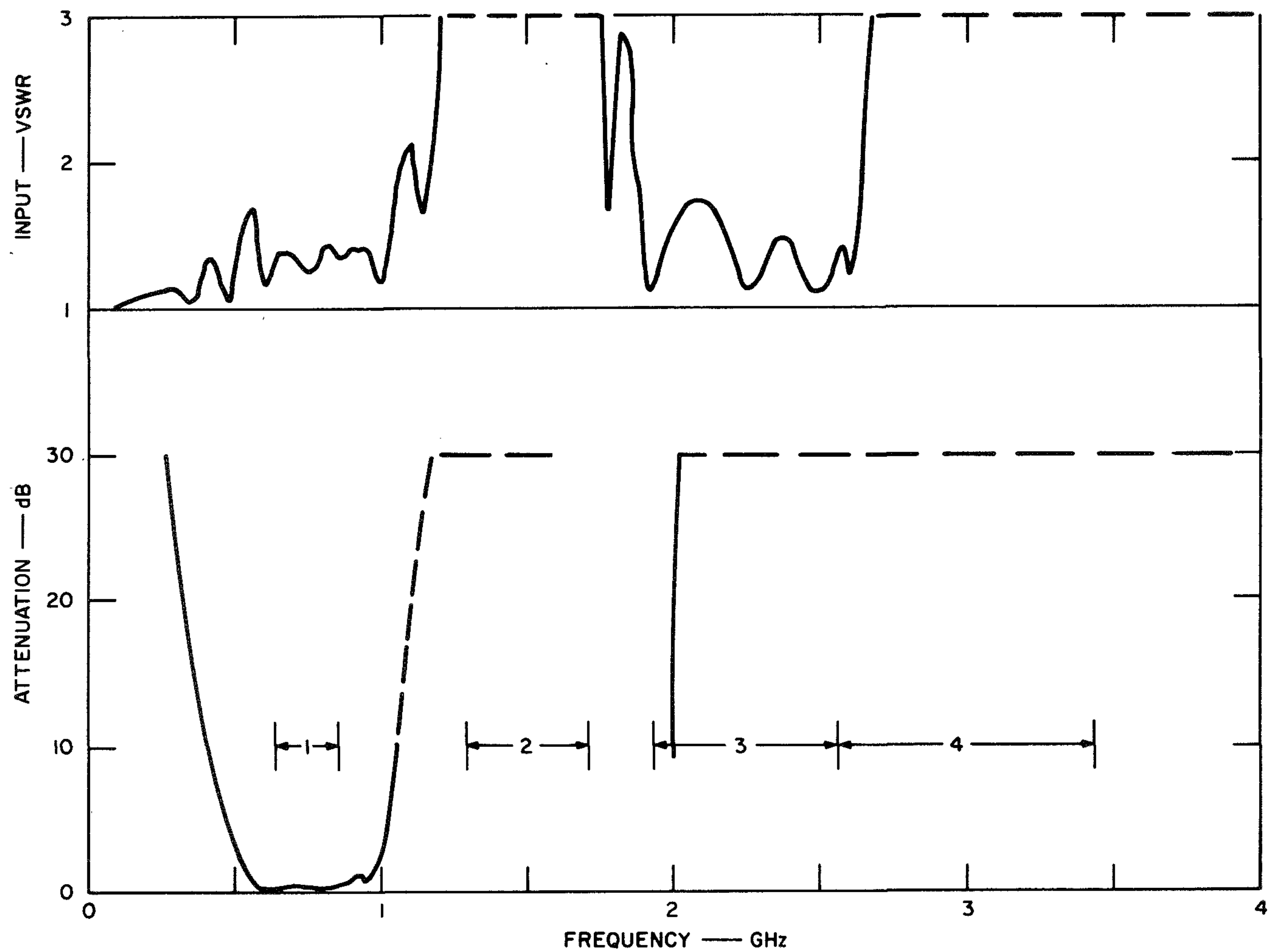

FIGURE 26 RESPONSE OF TRIPLEXER AFTER CONNECTING HARMONIC FILTERS. Input and Output ports are as in Figure 25.

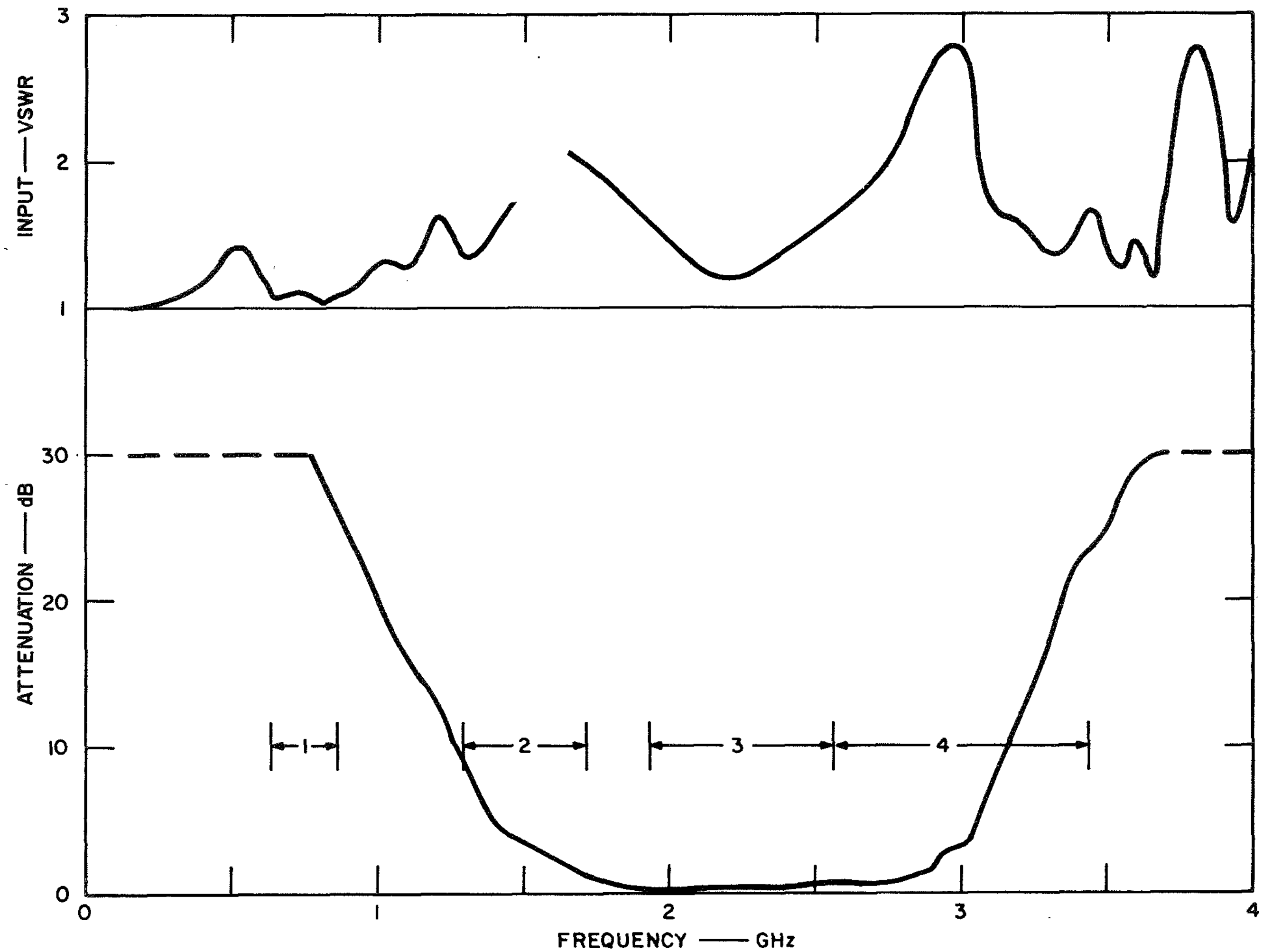

FIGURE 27 RESPONSE OF TRIPLEXER ONLY. Input is varactor port; Output is third harmonic port.

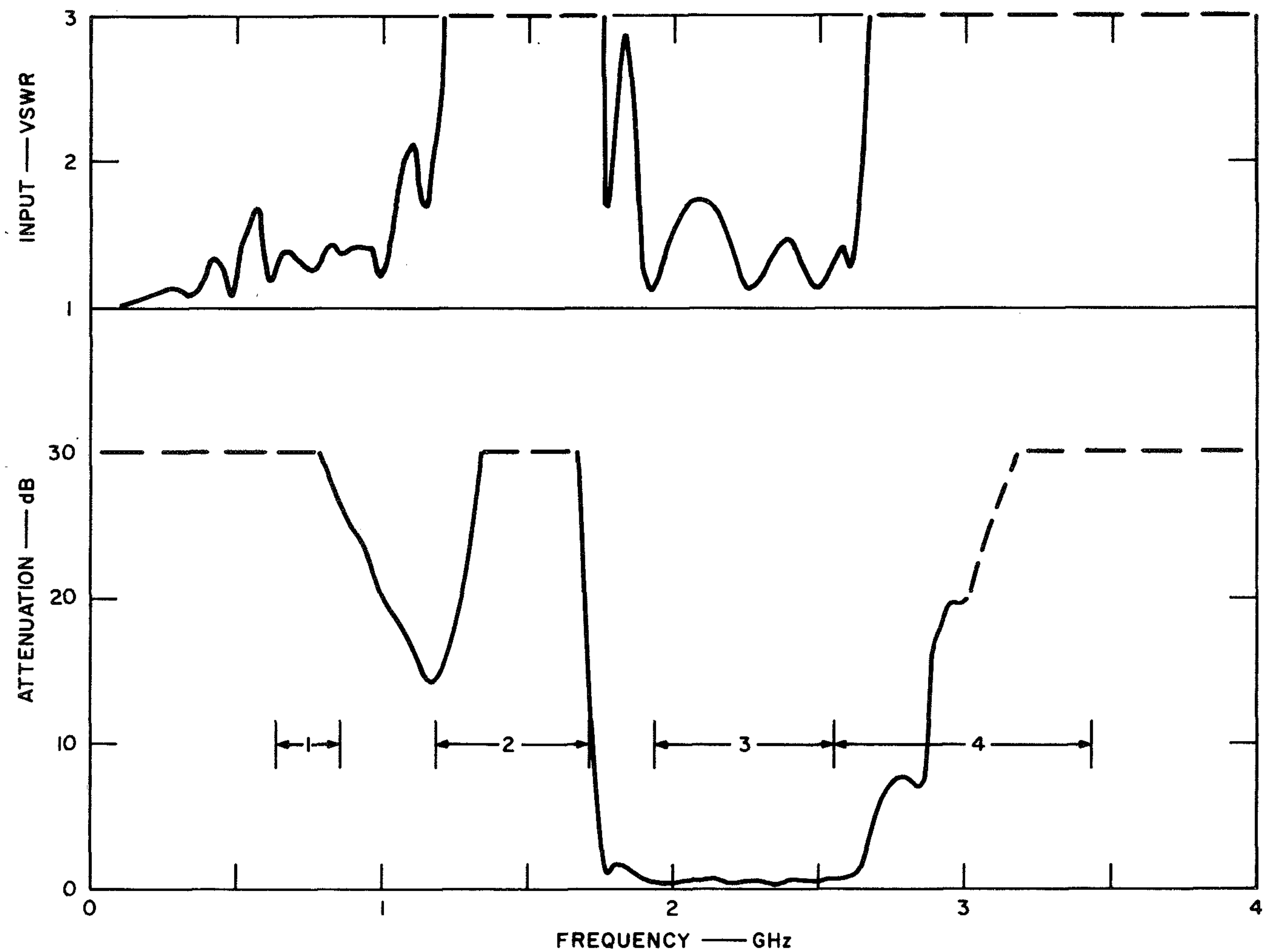

FIGURE 28 RESPONSE OF TRIPLEXER WITH HARMONIC FILTERS. Input and Output are as in Figure 27.

harmonic bandstop filters have been added, as in Figure 26. The pass band is now restricted essentially to the third harmonic band.

Isolation between the fundamental and third harmonic ports is shown in Figure 29, where the fundamental port is the input. The harmonic filters were not included in this test. Figure 30 shows the effect of adding the harmonic filters.

The purpose of the dummy load at the bandstop portion of the fundamental diplexer is to absorb energy in off-harmonic bands, especially in the subharmonic region, and in the region between the first and second harmonic bands. Figures 31 and 32 give the response from varactor port to dummy load, respectively, without and with the harmonic filters. Low VSWR and low attenuation are seen to occur in both regions of the frequency band.

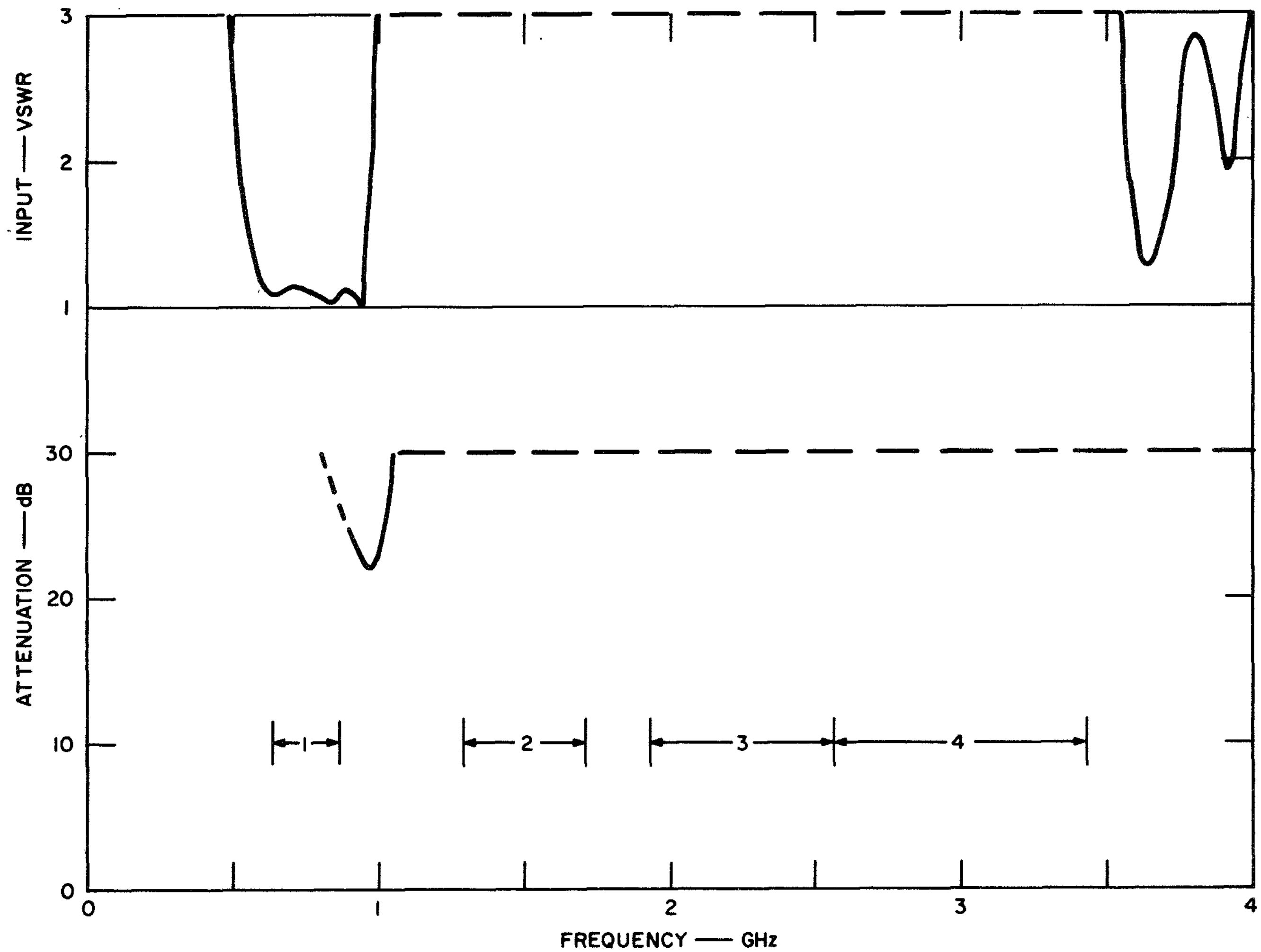

FIGURE 29 RESPONSE OF TRIPLEXER ONLY. Input is fundamental port; Output is third harmonic port.

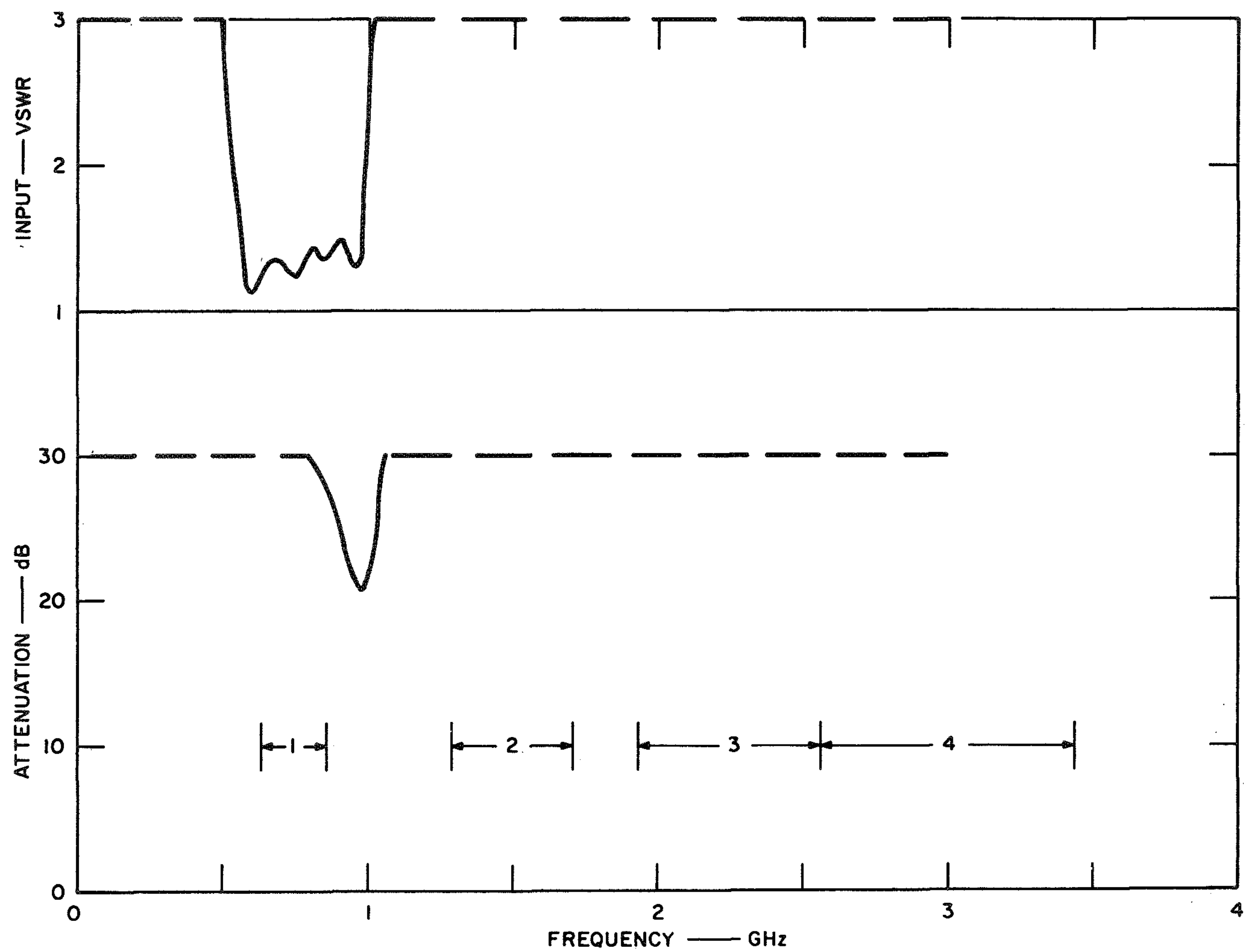

FIGURE 30 RESPONSE OF TRIPLEXER WITH HARMONIC FILTERS. Input and Output are as in Figure 29.

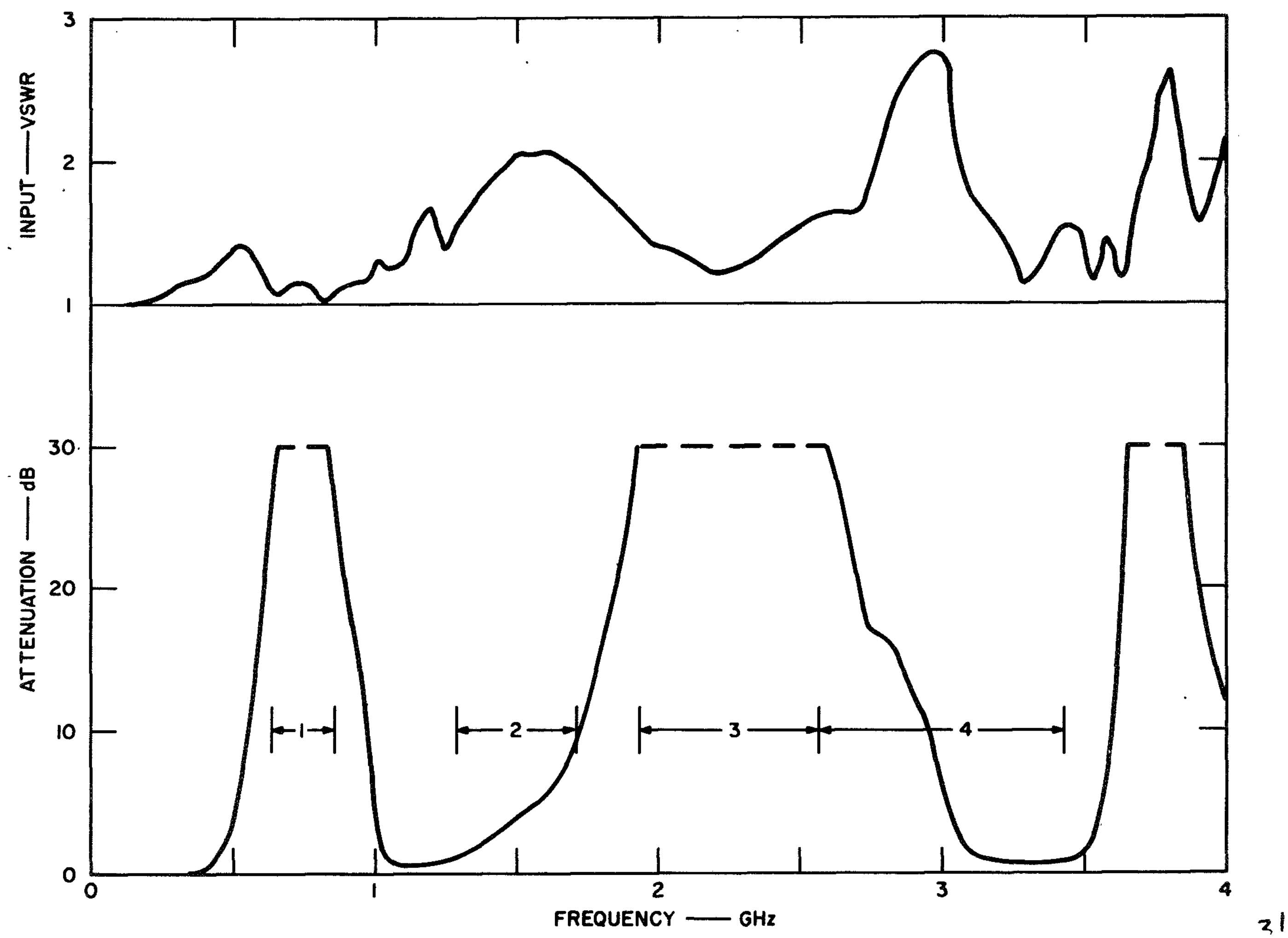

FIGURE 31 REPONSE OF TRIPLEXER ONLY. Input is varactor port; Output is dummy load port.

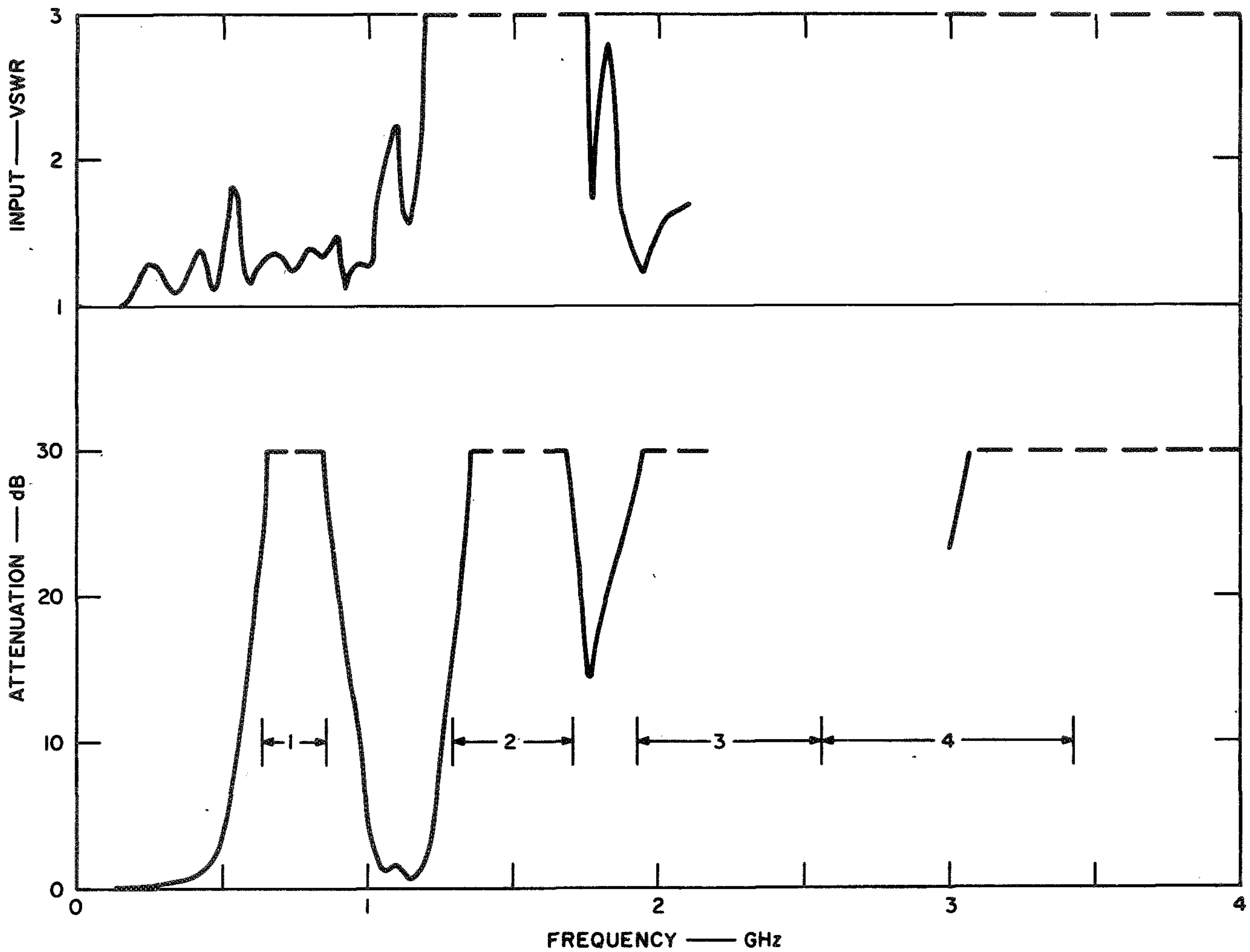

FIGURE 32 RESPONSE OF TRIPLEXER WITH HARMONIC FILTERS. Input and Output are as in Figure 31.

III MATCHING NETWORK CONSIDERATIONS

A. General

The design and construction of a suitable matching network between the diode and multiplexer are critical towards obtaining optimum tripler performance. The constraints on the matching network are severe, considerably more so than the conventional situation in which it is desired to efficiently transmit power from a resistive source to a passive complex load. The reason is that the matching network for a frequency multiplier must not only provide efficient power transfer, at the fundamental, but it must also present the proper impedances to the diode at each harmonic. Because of the nonlinearity of the frequency multiplication, the load impedances presented to the diode at all higher harmonics determines the diode input impedance at the fundamental. The condition of efficient power transfer is not identical to matching the impedances except for the singular case of a perfect match, as may be seen from the following analysis. For a lossless matching network the efficiency of power transfer to a complex load is given by

$$|S_{21}|^2 = 1 - |S_{11}|^2 \quad , \tag{8}$$

where

$$|S_{11}|^2 = \left| \frac{Z - Z_D^*}{Z + Z_D} \right|^2 \tag{9}$$

with

$Z = R + jX$ = impedance seen by the load looking into the matching network

$Z_D = R_D + jX_D$ = load impedance

Z_D^* = conjugate of Z_D.

Equation (9) may be rewritten in the form

$$(R - R_\alpha)^2 + (X + X_D)^2 = R_\beta^2 \quad , \tag{10}$$

where

$$R_\alpha = R_D \left\{ \frac{1 + |S_{11}|^2}{1 - |S_{11}|^2} \right\} \tag{11}$$

and

$$R_\beta = \frac{2|S_{11}|R_D}{1 - |S_{11}|^2} \quad .$$

Equation (10) represents the loci of constant power circles centered at $R = R_\alpha$, $X = -X_D$ with radii equal to $2|S_{11}|R_D/\left[1 - |S_{11}|^2\right]$. For a given value of $|S_{11}|$, all impedances Z satisfying Eq. (10) give identical power transfer to the diode.

Let us examine more carefully the implications of Eq. (10). The center of each constant power-transfer circle is at

$$X_C = X_D^*$$

$$R_C = R_D \left\{ \frac{1 + |S_{11}|^2}{1 - |S_{11}|^2} \right\}$$

and the circle radius is

$$R_\beta = \frac{2|S_{11}|R_D}{1 - |S_{11}|^2} \quad .$$

For perfect transmission, $|S_{11}| = 0$, which gives $R_C = R_D$, $X_C = X_D^*$ and $R_\beta = 0$. That is, a conjugate match is necessary for perfect transmission. For small mismatches, the centers of the circles shift only a little to the right, but the radii of the circles increase at a rate of $2R_D$. For large mismatches the centers of constant power-transmission circles move to the right substantially and the radii likewise become quite large. This is illustrated in Figure 33 for the case of a complex load $Z = 1 - j1$ and three values of $|S_{11}|$:

$|S_{11}| = 0.0$ (0 dB attenuation)

$|S_{11}| = 0.33$ (0.5 dB attenuation)

$|S_{11}| = 0.5$ (1.25 dB attenuation).

It can be seen from the figure that a mismatch of $|S_{11}| = 0.5$ can result in an impedance mismatch of 3:1, even though the efficiency of power transmission is still good, i.e., 75 percent. Even $|S_{11}| = 0.33$ (0.5 dB attenuation), which would normally be considered excellent efficiency, can result in an impedance mismatch of 2:1.

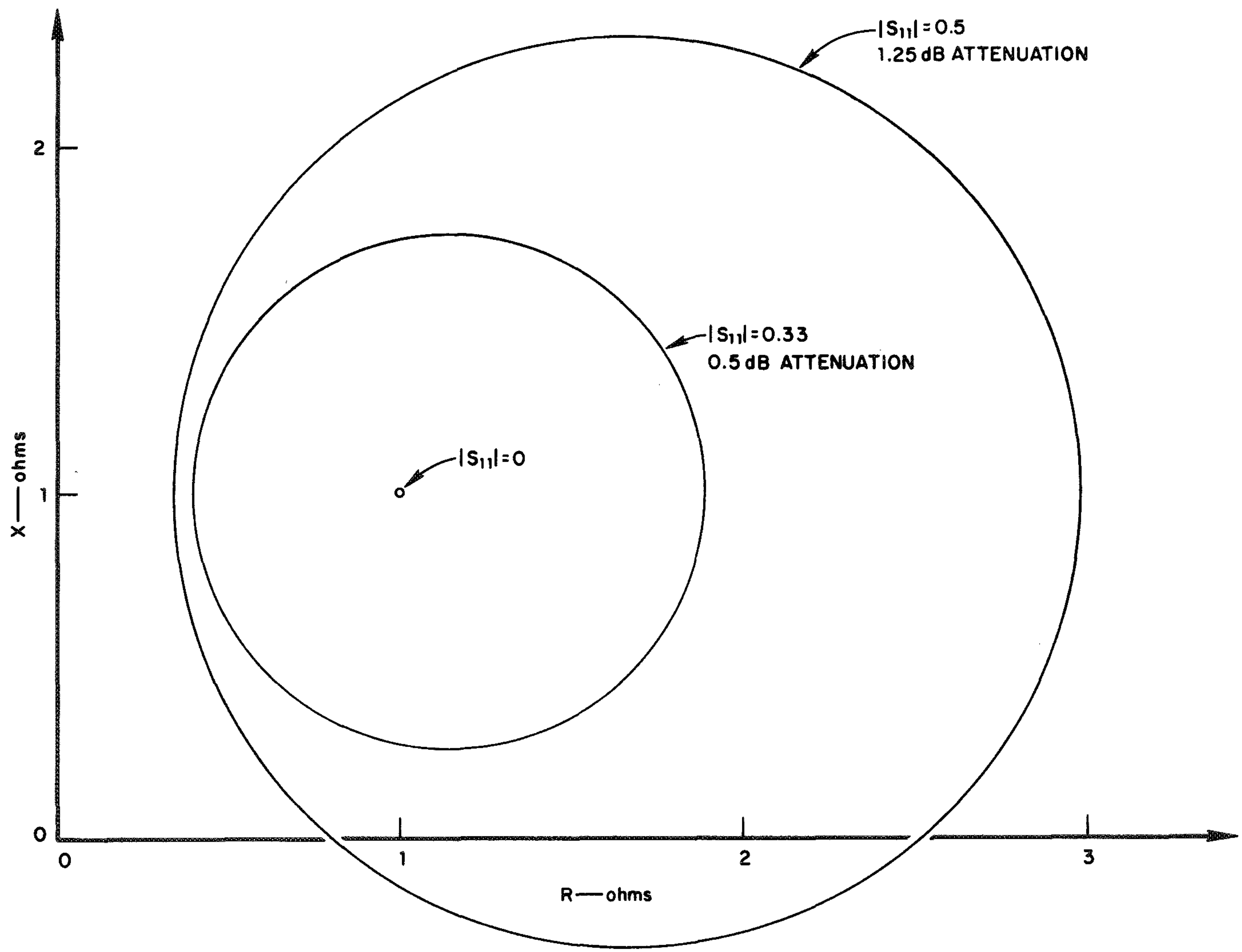

FIGURE 33 LOCI OF CONSTANT POWER TRANSFER TO A REACTIVE LOAD OF $Z = 1 - j1\ \Omega$

Thus, it is seen that, when considered from the point of view of tripler applications, the requirements on the matching network are stringent. An impedance mismatch of 3:1 or even 2:1 from the design impedances at the second or third harmonic could cause a severe mismatch of impedance at the fundamental. It is not known at this time the extent of impedance mismatch that can be tolerated at the second and third harmonics without significant degradation of tripler efficiency, but it seems reasonable to presume that 2:1 would seriously degrade the efficiency. Consequently, any proposed matching network at these harmonics should be substantially better than 0.5 dB.

B. Gain-Bandwidth Restrictions

Bode[13] and Fano[14] have stated the limitations on the matching of arbitrarily complex loads to resistive sources with lossless networks. These restrictions are conveniently stated in terms of a sequence of integral restrictions of the form

$$\int_0^\infty W_n(\omega)\ \ell n \left|\frac{1}{S_{11}}\right| d\omega \le C_n \qquad n = 1, 2 \ldots \tag{12}$$

where $W_n(\omega)$ is a positive weighting function for all ω and C_n is a positive finite constant associated with W_n. Equation (12) states that the area under the $W_n(\omega)\ \ell n \left|\frac{1}{S_{11}}\right|$ curve is finite. Consequently, the bandwidth over which a good match can be obtained is limited. Furthermore, a premium is paid for each point of perfect match since the integrand has a logarithmic singularity there. Clearly, in a band limited system, a flat loss is necessary in order to achieve the necessary bandwidth.

C. Design of the Matching Network

In designing matching networks at microwave frequencies, the practical limitations of component values and network realizability must be taken into consideration. For example, impedances of less than 5 and greater than 150 ohms are extremely difficult to realize in shielded TEM line. Consequently, only about a 30:1 range in impedance levels can be considered. Also, certain common filter structures, which might be used as matching networks, are limited in the transfer functions that they can realize. For example, half-wave parallel-coupled resonator filters can have only one transmission zero at infinity. For these reasons it was considered ill advised to attempt to find a theoretical solution to the matching problem. For, even if one could be obtained, there would be no guarantee that the filter could be physically realized at microwave frequencies. Therefore, the problem was approached in the following way:

(1) An arbitrary, but realistic, lumped network configuration was chosen that could be converted to a practical microwave network.

(2) The parameters of the network were adjusted by a systematic computer search and optimization program for a best match over the specified bandwidth.

A 4-resonator low-pass network was chosen for an initial starting network. The network was required to match the diode impedance over three bands: the fundamental, 700-800 MHz; the third harmonic, 2100 to 2400 MHz; and the second harmonic, 1400 to 1600 MHz. (It was necessary to match the diode to the second harmonic because it was assumed to have a small resistive component.) A ladder structure was chosen since this

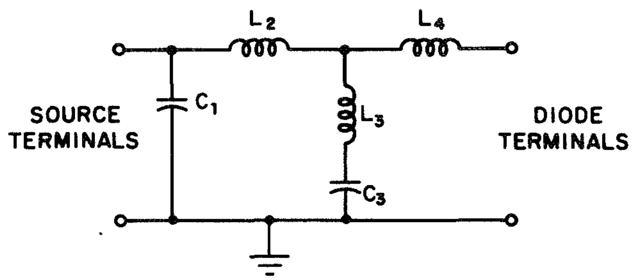

FIGURE 34 PROPOSED LOW-PASS DIODE MATCHING CIRCUIT

is readily converted to coaxial form. The network is shown in Figure 34. Impedance values for the diode were assumed to be:

Table VII

DIODE IMPEDANCE VALUES

Frequency Band	Diode Impedance (ohms)
Fundamental $f_{01} = 750$ MHz	$[25 - j31.2]\,\frac{f_{01}}{f}$
Second Harmonic $f_{02} = 1500$ MHz	$0.5 - j15.6\,\frac{f_{01}}{f}$
Third Harmonic $f_{03} = 2250$	$[9.14 - j10.2]\,\frac{f_{03}}{f}$

These impedances correspond to Steinbrecher's results for maximum efficiency.[15] The matching network was optimized over the above three bands, resulting in the following network parameters:

$$C_1 = 2.57 \text{ pF}$$

$$L_2 = 0.733 \text{ nH}$$

$$L_3 = 20.9 \text{ nH}$$

$$C_3 = 0.595 \text{ pF}$$

$$L_4 = 1.43 \text{ nH} \quad .$$

The attenuation between source and diode is shown in Figure 35. The match is approximately 1 dB in the fundamental and third harmonic bands, but sharply resonant in the second harmonic band. This result is not too surprising in view of stringent requirements asked of the 4-resonator low-pass network. In order to obtain a better match, the low-pass circuit should be triply resonated in order to meet all of the matching conditions in the three bands. While this is theoretically possible, the resulting structure would be quite complex, and not necessarily realizable. Furthermore, the gain-bandwidth restrictions previously described still hold, and it may yet be impossible to achieve a substantially better match over the present bandwidth. Recall that for efficient tripler operation, Figure 33 suggests that a match to within a few tenths of a dB is needed, and this quality of match may be completely incompatible with the present bandwidth.

D. Tripler Time-Domain Analysis

In order to theoretically analyze the efficiency of the tripler with the above matching network a generalized time-domain analysis computer program was used. The frequency dependence of the multiplexer was accounted for analytically in a fairly simple way that reduced computer running time. The diode was assumed to have an ideal punch-through characteristic. A bias level was chosen on the basis of the

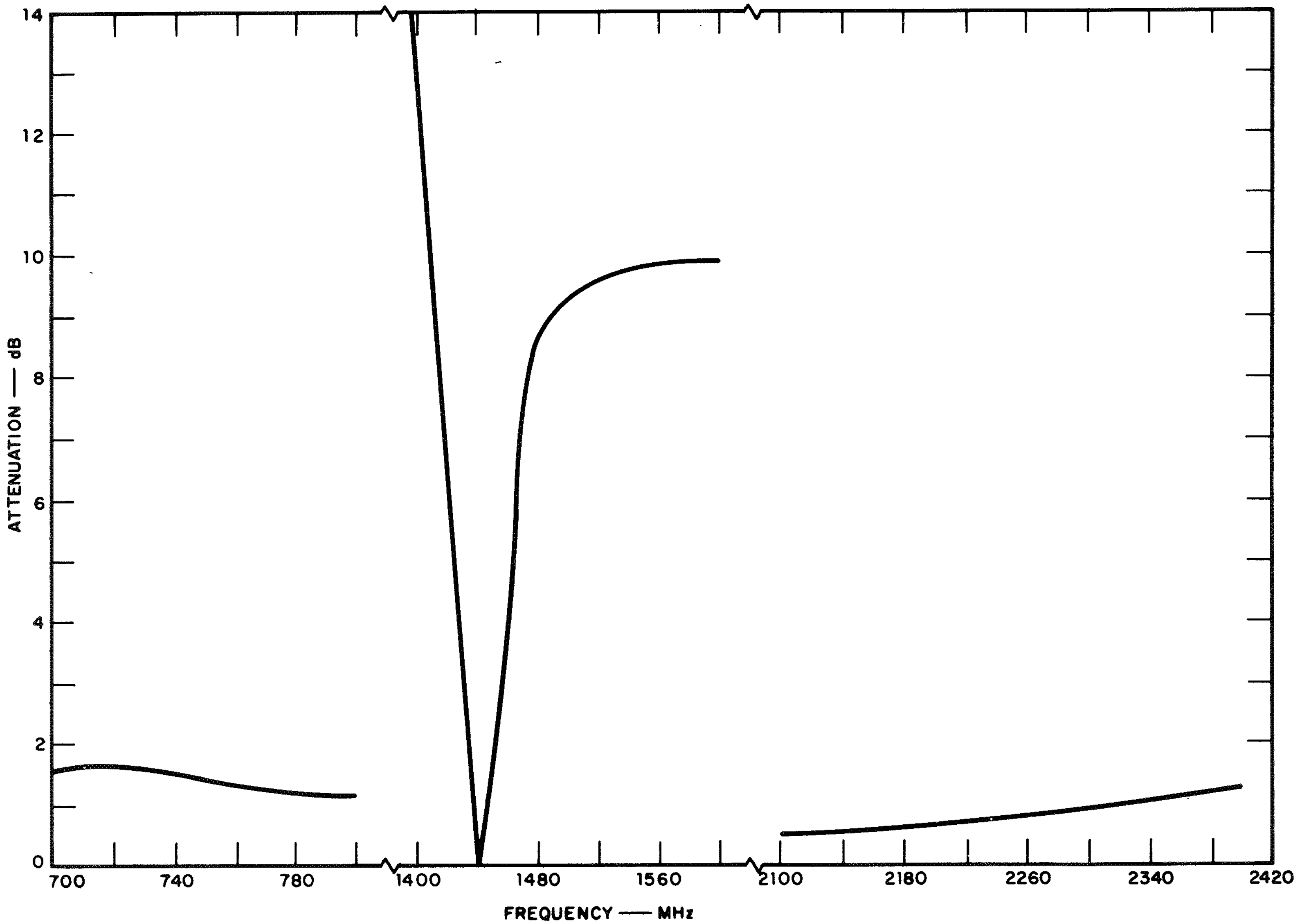

FIGURE 35 ATTENUATION RESPONSE OF MATCHING NETWORK

design curves of Steinbrecher[15] for triplers. The computer calculated the transient response for source frequencies of 700, 720, 740, 760, 780, and 800 MHz.* After the transient had settled down, the harmonic response was calculated using a fast-Fourier transform subroutine.

Figure 36 shows the VSWR at the source terminals. It is quite high, indicating substantial mismatch between the diode and source. This is not unexpected and is readily understood in terms of our previous discussion. For although the matching network was relatively efficient for the assumed passive complex load, it far exceeded the 0.1 to 0.3 dB match required for good tripler design. Consequently, the impedance of the diode at the fundamental was substantially different from that originally assumed because of the incorrect impedance terminations at the second and third harmonics. Figure 37 gives data of tripler efficiency defined as $P_{out}(f_3)/P_{avail}(f_0)$, and intrinsic diode efficiency, defined as

$$P_{out}(f_3)/[\text{Power delivered to diode at } f_0] \quad .$$

It is noteworthy that in the region in which the second harmonic is reactively terminated, although perhaps not optimally, the efficiency is highest. This strongly emphasizes the critical importance of the matching network in the current design approach. In conclusion, if the present tripler design approach is to be successful, a great deal of effort will be required to obtain matching networks that are realizable (in a practical sense) and can match the diode design impedances to within a few tenths of dBs.

---

* The data for 800 MHz are deleted in the following discussion because they were found in error. The harmonic analysis revealed that the steady state had not been reached when the harmonics were computed.

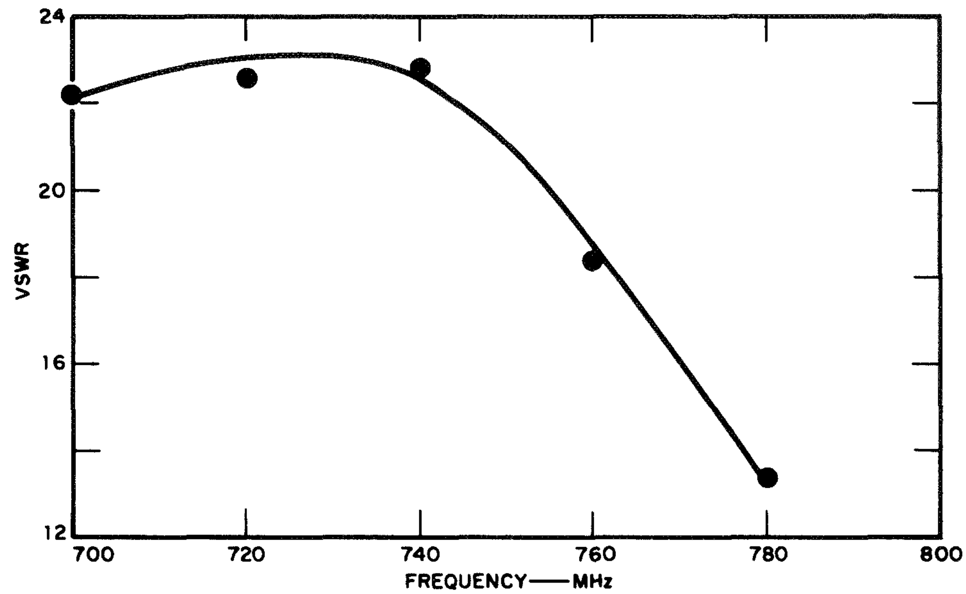

FIGURE 36 VSWR AT SOURCE TERMINALS

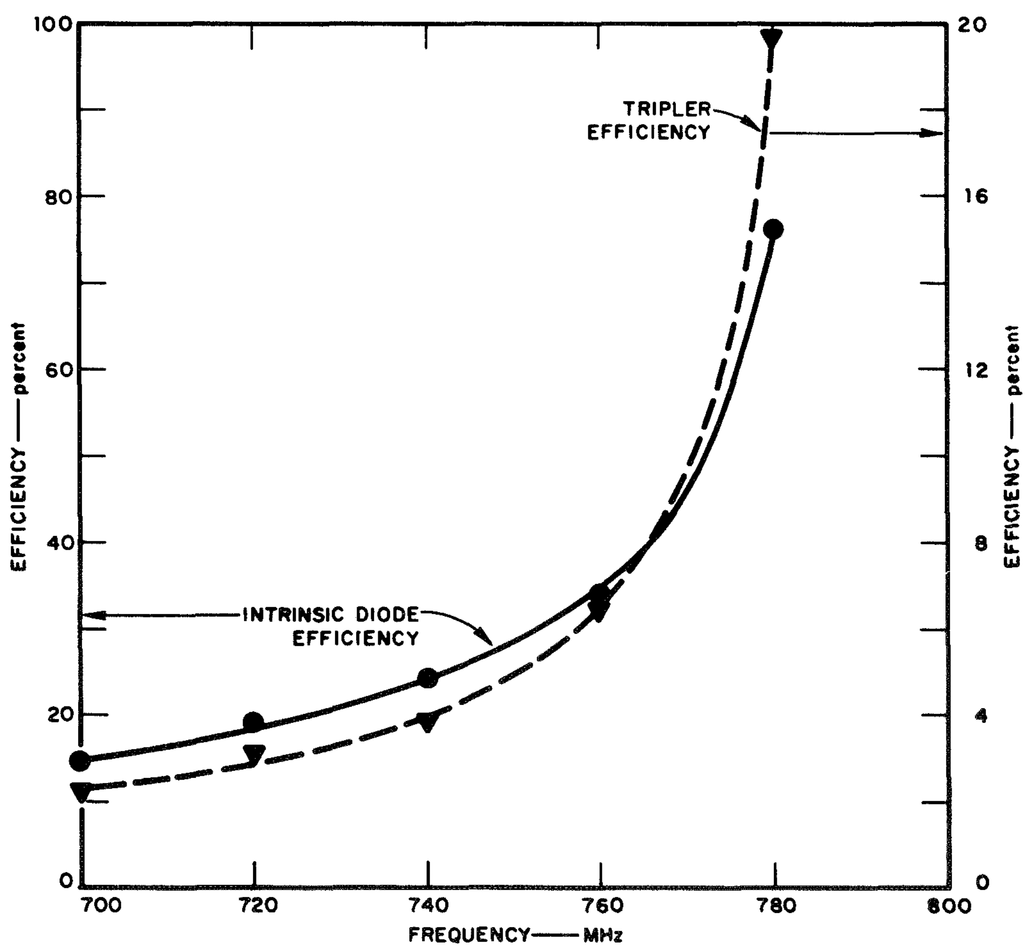

FIGURE 37 TRIPLER AND INTRINSIC DIODE EFFICIENCY

IV MEASUREMENTS ON AN EXPERIMENTAL TRIPLER

A diode mount was constructed for the Varian VAB 811A-EP bi-mode diode that was subsequently tested in the tripler hardware. The diode mount was connected in cascade with a coaxial line stretcher, second harmonic bandstop filter, and then the common port of the triplexer. Stub tuners were placed between the source and fundamental input and also between the third harmonic output detector and its respective port of the tripler. Power to the diode was 1.3 ± 0.1 watt. The tuners and line stretcher were adjusted for optimum efficiency and then the impedance seen from the diode terminals was measured on the SRI Automatic Network Analyzer. A representative result is shown in Figure 38. Figures 38(a), (b) and (c) show oscillographs of the impedances looking back into the tripler at the fundamental (697 MHz), the second and third harmonics, respectively. Normalized to 50 ohms these are

$$Z(f_0) = 0.19 + j.85$$

$$Z(2f_0) = 0.08 - j.13$$

$$Z(3f_0) = 0.55 - j.1 \quad .$$

At this frequency the tripler efficiency was 58 percent.

Efficiencies for source frequencies of 651 and 749 MHz were 34 and 41.5 percent, respectively. The tripler normalized output impedances for these frequencies were

$$Z(651) = 0.6 + j1.1$$

$$Z(1302) = 0.05 - j.08$$

$$Z(1953) = 0.9 + j.18$$

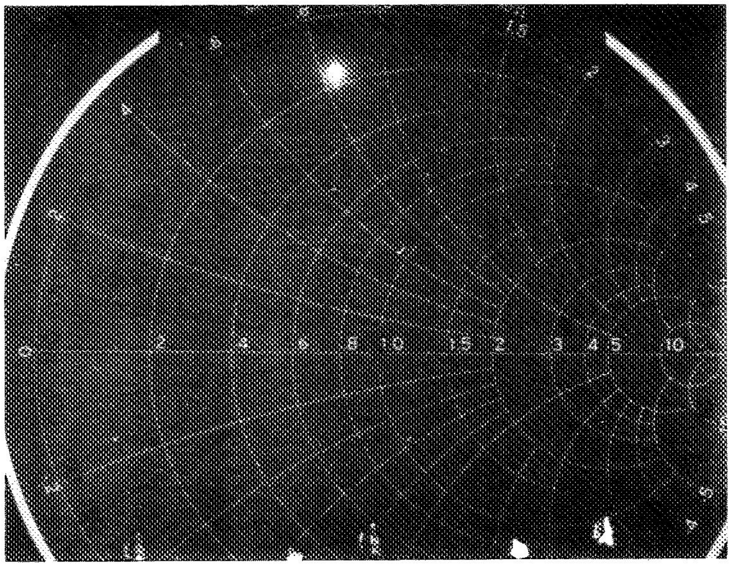

(a) Z AT 697 MHz

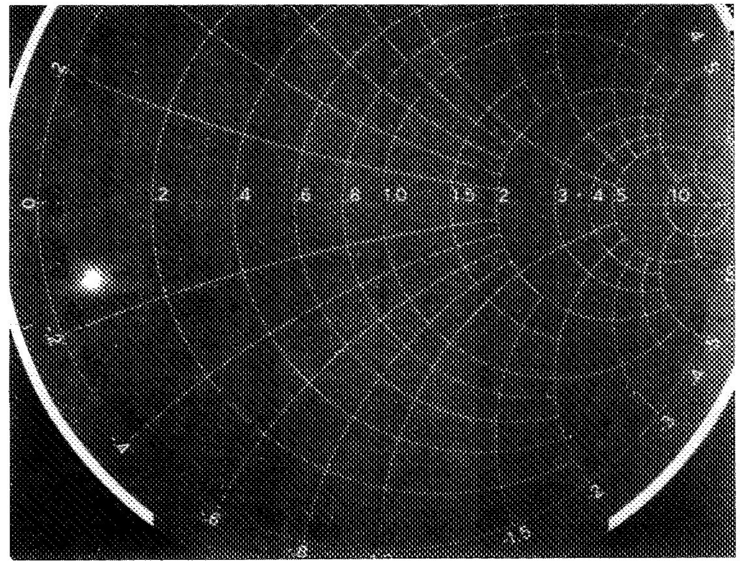

(b) Z AT 1394 MHz

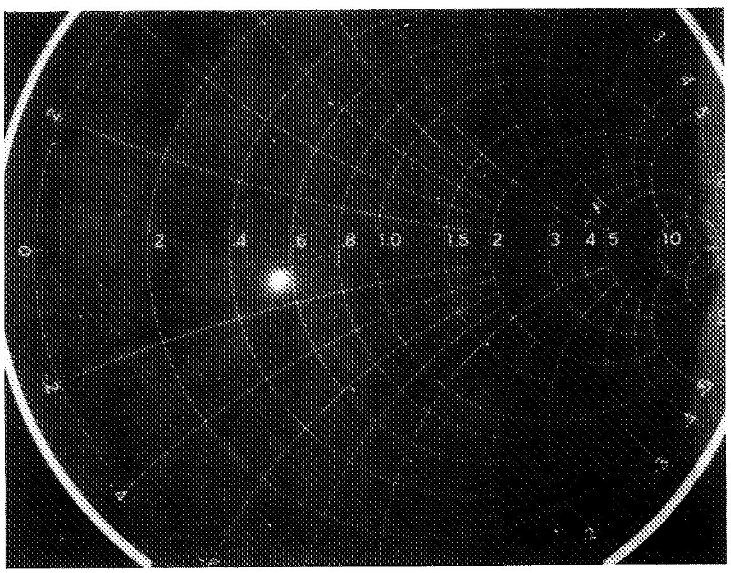

(c) Z AT 2091 MHz

FIGURE 38 MEASURED TRIPLER OUTPUT IMPEDANCES FOR A SOURCE FREQUENCY OF 697 MHz and

$$Z(749) = 0.7 + j.9$$

$$Z(1498) = 0.02 + j.4$$

$$Z(2247) = 0.38 + j.05 \quad .$$

Measurements were also taken at 800 and 850 MHz. However, these have since been found to be erroneous, and there was insufficient time to retake these data for this report.

V CONCLUSIONS

The triplexer attenuation and common port VSWR response were generally satisfactory. The largest component of the triplexer was the channel-dropping-filter for the source frequency. Its size could be substantially reduced by realizing the same electrical design with semi-lumped elements. The bandstop filters for the second and fourth harmonic bands are better incorporated in the matching filter rather than as individual components. In this way the triplexer is made more compact and redundancy of components is reduced.

The efficiency of triplexers of the present design depends critically on the tolerance of match between the diode and the triplexer. The matching network must present the correct impedances to the diode at the second and third harmonics and match the diode impedance at the fundamental. Analysis showed that the tolerance of match required for the second and third harmonic bands (in terms of power-transfer efficiency) is certainly less than 0.5 dB, and probably as small as 0.1 or 0.2 dB. This is extremely difficult to achieve over wide bandwidths and will require complex matching circuits in order to cover the three frequency bands (i.e., the fundamental, second, and third harmonics). The practical realization of microwave matching structures adds another degree of difficulty to the overall matching problem. For these reasons, a substantial part of any future tripler work using this design approach should be directed to the solution of the matching network problem.

If the tolerance of match cannot be reduced to sufficiently small values over the required bandwidths, because of either theoretical or practical limitations, it is recommended that the matching network be be optimized in the time-domain. Time-domain optimization has the distinct advantage that the matching network and tripler efficiency are optimized in a self-consistent manner. Indeed, this may be the only way to efficiently solve the wideband tripler case.

REFERENCES

1. A. I. Grayzel and R. T. Minkoff, "A New Technique for Designing Highly-Stable High-Efficiency Varactor Multiplier Chains, Digest of the 1969 G-MTT International Symposium, Dallas, Texas, 5-7 May 1969, pp. 131-6.

2. R. Wenzel, "Application of Exact Synthesis Methods to Multi-Channel Filter Design," IEEE Trans. on Microwave Theory and Techniques, Vol. MTT-13, pp. 13, pp. 5-15 (January 1965).

3. G. L. Matthaei, L. Young, and E.M.T. Jones, Microwave Filters, Impedance-Matching Networks and Coupling Structures, p. 985 (McGraw-Hill, New York, 1964).

4. H. Ozaki and J. Ishii, "Synthesis of a Class of Strip-Line Filters," IRE Trans. on Circuit Theory, Vol. CT-5, pp. 104-109 (June 1958).

5. E. G. Cristal, "Addendum to an Exact Method for Synthesis of Microwave Band-Stop Filters," IEEE Trans. on Microwave Theory and Techniques, Vol. MTT-12, pp. 369-382 (May 1964).

6. B. M. Schiffman and G. L. Matthaei, "Exact Design of Bandstop Microwave Filters," IEEE Trans. on Microwave Theory and Techniques, Vol. MTT-12, pp. 6-15,(January 1964).

7. W. J. Getsinger, "Coupled Rectangular Bars Between Parallel Plates," IRE Trans. on Microwave Theory and Techniques, Vol. MTT-10, pp. 65-72 (January 1962).

8. R. J. Wenzel, "Exact Theory of Interdigital Band-Pass Filters and Related Coupled Structures," IEEE Trans. on Microwave Theory and Techniques, Vol. MTT-13, pp. 559-575 (September 1965).

9. E. G. Cristal, "Coupled Cylindrical Rods Between Parallel Ground Planes," IEEE Trans. on Microwave Theory and Techniques, Vol. MTT-12, pp. 428-439 (July 1964).

10. S. B. Cohn, "The Reentrant Cross Section and Wide-Band 3-dB Hybrid Couplers," IEEE Trans. on Microwave Theory and Techniques, Vol. MTT-11, pp. 254-258 (July 1963).

11. R. Saal, "The Design of Filters Using the Catalogue of Normalized Low-Pass Filters," Telefunken G.M.B.H., Backnang/Württ, West Germany, 1963.

12. M. C. Horton and R. J. Wenzel, "The Digital Elliptic Filter," IEEE Trans. on Microwave Theory and Techniques, Vol. MTT-15, pp. 307-314 (May 1967).

13. H. Bode, Network Analysis and Feedback Amplifier Design (D. Van Nostrand and Company, New York, 1945).

14. R. M. Fano, "Theoretical Limitations on the Broadband Matching of Arbitrary Impedances," J. Franklin Inst., Vol. 249, pp. 57-83 and 139-154 (January and February 1950).

15. D. H. Steinbrecher, "Efficiency Limits for Tuned Harmonic Multipliers with Punch Through Varactors," Digest of Technical Papers, 1967 International Solid State Circuits Conference, 15-17 February 1967 pp. 20-21.